J. Fluid Mech. (2004), *vol.* 516, *pp.* 83–113.
DOI: 10.1017/S0022112004000473 Printed in the United Kingdom

A laboratory study of localized boundary mixing in a rotating stratified fluid

By J. R. WELLS† AND K. R. HELFRICH

Department of Physical Oceanography, Woods Hole Oceanographic Institution, Woods Hole, MA 02543, USA

(Received 11 December 2003 and in revised form 20 April 2004)

Oceanic observations indicate that abyssal mixing tends to be localized to regions of rough topography. How localized mixing interacts with the ambient fluid in a stratified, rotating system is an open question. To gain insight into this complicated process laboratory experiments are used to explore the interaction of mechanically induced boundary mixing and an interior body of linearly stratified rotating fluid. Turbulence is generated by a single vertically oscillating horizontal bar of finite horizontal extent, located at mid-depth along the tank wall. The turbulence forms a region of mixed fluid which quickly reaches a steady-state height and collapses into the interior. The mixed-layer thickness, $h_m \sim \gamma(\omega/N)^{1/2}$, is spatially uniform and independent of the Coriolis frequency f. N is the initial buoyancy frequency, ω is the bar oscillation frequency, and $\gamma \approx 1$ cm is an empirical constant determined by the bar geometry. Surprisingly, the export of mixed fluid does not occur as a boundary current along the tank perimeter. Rather, mixed fluid intrudes directly into the interior as a radial front of uniform height, advancing with a speed comparable to a gravity current. The volume of mixed fluid grows linearly with time, $V \propto (N/f)^{3/2} h_m^3 ft$, and is independent of the lateral extent of the mixing bar. Entrainment into the turbulent zone occurs principally through horizontal flows at the level of the mixing that appear to eliminate export by a geostrophic boundary flow. The circulation patterns suggest a model of unmixed fluid laterally entrained at velocity $u_e \sim N h_m$ into the open sides of a turbulent zone with height h_m and a length, perpendicular to the boundary, proportional to $L_f \equiv \gamma(\omega/f)^{1/2}$. Here L_f is an equilibrium length scale associated with rotational control of bar-generated turbulence. The model flux of exported mixed fluid $Q \sim h_m L_f u_e$ is constant and in agreement with the experiments.

1. Introduction

Turbulent mixing in the deep ocean is fundamental to the meridional overturning circulation. Cold dense bottom water, formed through surface heat loss in high-latitude marginal seas, sinks, spreads equatorward and upwells in the ocean basins. To complete the overturning cycle and to sustain the steady-state density distribution of the world oceans, the rising water must be modified by the downward diffusion of heat. Munk (1966) proposed a one-dimensional advective–diffusive balance to account for the distribution of temperature and salinity in the central Pacific. In this model the upwelling of Antarctic Bottom Water implied a constant diapycnal mixing rate with the turbulent diffusivity coefficient $\kappa \approx 10^{-4}\,\mathrm{m^2\,s^{-1}}$. Hogg *et al.* (1982), in

† Present address: Center for Coastal Physical Oceanography, Old Dominion University, Norfolk, VA 23529, USA

a mass and heat budget of the Brazil Basin, inferred a similar spatially averaged mixing rate of $O(10^{-4})\,\mathrm{m^2\,s^{-1}}$. Locally observed mixing rates, however, range over three orders of magnitude. Microstructure measurements and tracer studies show that in the ocean interior away from boundaries diffusivities are $O(10^{-5})\,\mathrm{m^2\,s^{-1}}$, while over abrupt topographic features mixing rates climb as high as $10^{-3}\,\mathrm{m^2\,s^{-1}}$ (Lueck & Mudge 1997; Polzin *et al.* 1997; Toole, Polzin & Schmitt 1994; Toole, Schmitt & Polzin 1997; Ledwell *et al.* 2000). The distribution pattern suggests that locally generated salinity and temperature characteristics are exported from mixing sites along neutral surfaces and that the advective–diffusive balance is a three-dimensional rather than a one-dimensional process (Munk & Wunsch 1998).

Few observations exist of the interactions between turbulent regions and ambient ocean waters, but in the laboratory aspects of the dynamics can be isolated and explored. The research described in this paper considers both horizontal and vertical exchanges between a localized patch of mixing and a quiescent body of rotating stratified fluid. The experiments are conducted in a rotating tank filled with linearly stratified salt water. Turbulence is induced by a single oscillating bar of finite width placed at mid-depth along a section of the tank wall. The experiments investigate the entrainment of ambient fluid into the turbulent zone, the export of mixed fluid into the interior of the tank, mixed fluid properties, volume and distribution, and the overall flow field associated with localized mixing. These characteristics are described and quantified as functions of the Coriolis frequency,

$$f = 2\Omega, \tag{1}$$

where Ω is the tank rotation rate about the vertical z-axis, and the buoyancy frequency, N,

$$N^2 = -\frac{g}{\rho_o}\frac{\partial \rho}{\partial z}, \tag{2}$$

where g is the acceleration due to gravity, ρ_o is the reference density, and $\rho(z)$ is the ambient density. Turbulent properties are described as a function of the bar oscillation frequency, ω. The parameterization of bar-generated turbulence is discussed in § 3.

Oceanic observations suggest that the energy for local turbulent mixing comes from internal waves that arise from tidal flow over rough topography, interact and develop instabilities (Ledwell *et al.* 2000). In the laboratory it is difficult to produce sustained controlled mixing through a similar process. Since the goal is to examine the effects, rather than the source, of localized mixing, the experiments rely on a mechanical mixing method to establish turbulence. Previous laboratory studies have examined the properties of mechanically induced turbulence and its evolution in the presence of stratification or rotation, and provide a background for the parameterization of bar-induced turbulence developed in § 3.

The present research also builds upon laboratory studies that investigated the interaction of mechanically generated mixing with a rotating stratified environment. Ivey (1987) considered vertical boundary mixing, Thomas & Linden (1996) examined cross-frontal exchanges, and Davies *et al.* (1991) studied the effects of mixing at the end of a channel.

Ivey (1987) imposed turbulence in a two-layer fluid using a centrally placed, vertically oscillating cylindrical grid of spaced horizontal bars. While the grid generated turbulence over the full depth of the tank, mixing was restricted to the density interface. Mixed fluid moved radially outward along the neutral density surface and developed into an anticyclonic rim current around the grid which

ultimately became unstable. The resulting chaotic eddy field transported mixed fluid further into the basin interior. Ivey found that rotation was a factor in the width of the coherent boundary current and the onset of instability, and thus affected the horizontal distribution of mixed fluid. However, the vertical mixing rate was independent of rotation and solely a function of stratification and grid frequency.

Thomas & Linden (1996) produced mixing across a horizontal density gradient. The mixing mechanism was a horizontally oriented, vertically oscillating flat circular grid in the centre of a cylindrical tank initially filled with a two-layer system. The mixing established a central full-depth column of intermediate-density fluid which spread radially along the neutral density surface. Once the mixed layer reached the outer tank wall, mixed-layer height began to increase. By observing volume changes in the three layers Thomas & Linden found that the growth of the mixed layer was governed by the rate at which ambient fluid could enter the central mixing zone, and that this was affected by rotation. Horizontal entrainment increased with stratification and decreased with rotation.

Davies *et al.* (1991) imposed mixing at one end of a long rotating rectangular tank filled with linearly stratified salt water. The mixer, a vertically oscillating horizontal grid of intersecting bars, spanned the width of the tank. The arrangement was distinct from the previously described full-depth axisymmetric mixing mechanisms. Davies *et al.* observed the vertical growth of the turbulent layer at the grid and the horizontal circulation of the outflow of mixed fluid. The outflow was deflected to the right, forming a boundary current that followed the tank perimeter. After the initial development phase, the mixed-layer thickness near the grid remained constant until the boundary current returned to the source, after which it resumed thickening. While the initial mixed-layer height was determined by stratification, the further growth after the return of the boundary current was an increasing function of rotation. Davies *et al.* concluded that vertical entrainment was being augmented over long times by the lateral injection of previously mixed fluid.

It is interesting that turbulent entrainment of ambient fluid in the Ivey, Thomas & Linden, and Davies *et al.* experiments appears to depend as much on the configuration of the mixing region as on variations in stratification and rotation. The structure of the mixing region in each case determined the possible pathways of fluid exchange and influenced the roles of rotation and stratification in the production of mixed fluid.

In this work a single bar of finite horizontal length is used to generate turbulent mixing at the boundary of a rotating cylindrical tank of linearly stratified fluid. The localized nature of the turbulence permits both vertical and horizontal entrainment of ambient fluid and distinguishes these experiments from the earlier studies. Based on the experiments cited above, stratification was expected to limit the height of the mixed layer and the mixed outflow was expected to form a geostrophic boundary current that flowed around the tank perimenter. The experiments do show a single mixed layer of uniform thickness and finite width moving out from the bar. Surprisingly, the emerging intrusion does not form a cyclonic boundary current. Instead, flows exiting the turbulent region appear to be constrained by entrainment-driven horizontal flow approaching the region. The mixed fluid moves directly into the interior as a broad front until the coherent advance gives way to instability. The subsequent distribution of mixed fluid is through baroclinic eddies. The lateral entrainment of ambient fluid at the level of the turbulent zone dominates the vertical entrainment.

Section 2 describes the laboratory apparatus and measurement techniques. Section 3 discusses the bar-induced turbulent properties, and defines length scales used in the

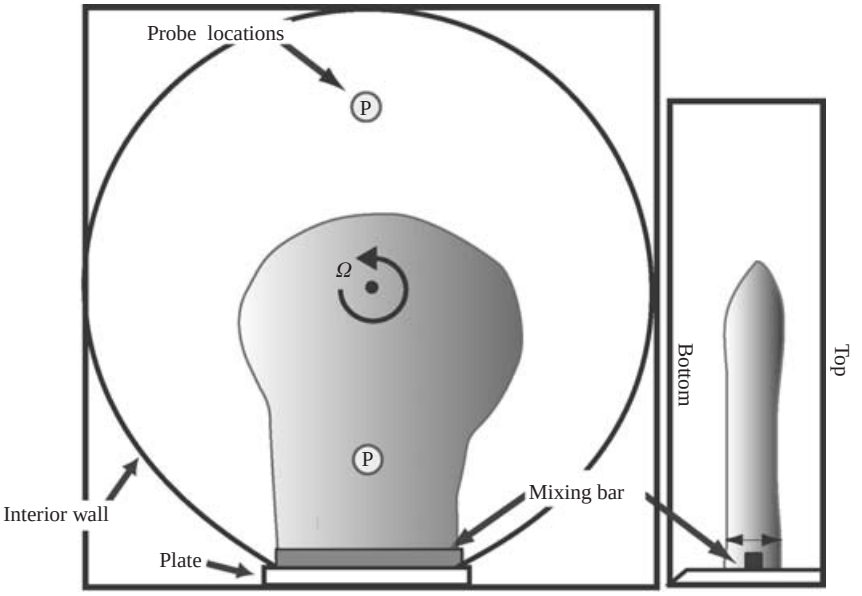

FIGURE 1. Sketch of the experimental apparatus, showing a top view of the 114×114 cm square glass tank, the circular interior wall, the probe locations, and the mixing bar and support plate. To the right of the tank is a 45° mirror giving a side view of the bar. The mixed fluid is shown moving directly out from the bar. Its area is measured from the top view; the height is measured from the mirror view at the site of the doubleheaded arrow.

analysis of experimental results. Sections 4 and 5 give a qualitative picture of the exchanges between the turbulent patch and the basin interior, and a quantitative analysis of the production of mixed fluid, respectively. Section 6 proposes a simple scaling model that ties the volume flux of mixed fluid to the lateral entrainment process. Section 7 examines variations in the width of the mixing bar. Section 8 investigates the limits of rotational effects on mixed-fluid flux. The concluding section summarizes the laboratory results and examines their application to oceanic mixing.

2. Experimental set-up

2.1. *Laboratory apparatus*

A sketch of the laboratory apparatus is given in figure 1. The $114 \times 114\,\mathrm{cm}^2$ glass tank was fitted with an interior circular Plexiglas false wall forming a cylindrical working section that prevented corner effects from complicating interior flows. The adjacent 45° mirror was used to give side views of the experiments when viewed from above. The entire apparatus was placed on a 2 m diameter turntable. Both the table and a video camera, located 5 m above the tank, rotated with angular frequency $\Omega = f/2$ (counterclockwise when viewed from above). The tank was filled with linearly stratified salt water to a working depth of 26.5 cm.

Turbulent mixing was produced by vertically oscillating a single horizontal bar with a fixed cross-section, $1.27 \times 1.27\,\mathrm{cm}^2$, and a variable width, $15 \leqslant L_B \leqslant 30$ cm. The motion was sinusoidal with amplitude, $A = 0.35$ cm, and frequency, $\omega = [7, 14, 28]\ \mathrm{s}^{-1}$. Figure 1 shows the bar mounted at mid-depth on a support plate which was set into a flat section of the interior wall. The support plate did not introduce any additional

mixing except at its lower edge. This disturbance was minimized by chamfering the bottom of the plate.

The main visual record of the flow was obtained by the injection of dye directly in front of the bar. The dye injection system used a syringe pump and several narrow gauge needles to introduce dye continuously and evenly. The dye was mixed quickly throughout the turbulent region and marked the subsequent movement of mixed fluid. The overhead video camera photographed the top view and the reflected side view of the spreading dye. These images were recorded on both video tape and in directly digitized computer image sequences with known time intervals.

The initial stratification was measured using a Precision Measurement Engineering conductivity probe, calibrated for each experiment. In addition, periodic vertical profiles of the conductivity were used to monitor the temporal evolution of the stratification. Vertical profiles of conductivity measurements were made from approximately 5 cm beneath the rigid lid (see below) to within 2 cm of the sand bottom at 19 and 94 cm in front of the bar.

2.2. *Stratification and spin-up*

The linear stratification was accomplished through the two-reservoir method (Oster 1965). Increasingly dense water was introduced over a 2 hour period through a diffuser at the bottom of the tank that was covered by a layer of sand. The sand helped speed up the spin-up.

For a linearly stratified fluid the spin-up time is $\tau = O(H^2/\nu)$, where H is the total depth and $\nu = 0.01\,\mathrm{cm^2\,s^{-1}}$ is the kinematic viscosity of water. However, rigid-body rotation cannot be achieved in a stratified laboratory container, regardless of the elapsed time. The pressure surfaces of the fluid form paraboloids of revolution. Because of the no-salt-flux condition at the vertical tank walls the density surfaces are not parallel with the pressure surfaces. Thus the horizontal density gradient along the pressure surfaces induces an azimuthal flow (Barcilon & Pedlosky 1967).

A balance was sought in the spin-up process between the time required for the fluid to come into approximately solid-body rotation with the container, and the time within which diffusive processes at the tank perimeter induce a background flow. An early set of experiments investigated the spin-up for a free surface and for a rigid lid with $N = 0.7\,\mathrm{s^{-1}}$ and $f = [0.3, 0.7, 1.4]\,\mathrm{s^{-1}}$. The horizontal displacements of vertical streaks from potassium permanganate crystals were monitored over a 6 hour period after the tank was filled. The free-surface experiments showed azimuthal anticyclonic residual velocities increasing linearly from zero at the bottom boundary to a maximum of $O(10^{-1})\,\mathrm{cm\,s^{-1}}$ at the free surface. Within the first four hours the flows decreased by about one half, and over the following two hours the decay process continued, though more slowly. With the addition of the rigid lid azimuthal velocities peaked at mid-depth and decreased to zero at the top and bottom boundaries. The velocity maxima were reduced by half.

All the rotating experiments discussed below were conducted using a rigid lid. A piece of Plexiglas was placed over the interior circular portion of the tank. It was supported by styrofoam floats and rose with the incoming fluid. Four to six hours after the tank was filled and prior to the initiation of mixing, the background velocity field was checked. Velocity magnitudes were $O(10^{-2})\,\mathrm{cm\,s^{-1}}$, negligible with respect to the mixing-induced circulations, and the vertical structure and horizontal direction of the flow showed no distinct pattern. The rigid lid also served to eliminate surface waves generated by the vertical motion of the mixer.

2.3. *Experimental variables*

The primary independent variables were the buoyancy frequency N, Coriolis frequency f, and bar oscillation frequency ω. These were varied over the ranges $N = [0, 0.21, 0.35, 0.70]\,\mathrm{s}^{-1}$ and $f = [0, 0.35, 0.70, 1.40]\,\mathrm{s}^{-1}$, giving $\frac{1}{4} \leqslant N/f \leqslant 3$, and $\omega = [7, 14, 28]\,\mathrm{s}^{-1}$. In all cases the bar frequency was much higher than the buoyancy and Coriolis frequencies, ω/N, $\omega/f \gg 1$. Bar motion created localized turbulent mixing rather than internal or inertial waves. The horizontal extent of the mixing region was controlled by the bar width, $L_B = [15.2, 20.3, 22.9, 30.5]\,\mathrm{cm}$, which was kept much smaller than the inner tank diameter, $L_t = 112\,\mathrm{cm}$. The short bar and the mid-depth location left the mixing region exposed to both lateral and vertical exchanges with the ambient fluid.

3. Mechanically generated turbulence

3.1. *Background*

The parameterization developed for bar-induced turbulence follows from the Hopfinger & Toly (1976) model of the spatial decay of grid-generated turbulence and from similar experimental studies of the inhibition of turbulence by buoyancy. Hopfinger & Toly (1976) generated turbulence in a non-rotating homogeneous fluid through vertical oscillation of a horizontally planar grid of intersecting bars. Direct measurements of the r.m.s. velocity, u_t, and the integral length scale, l_t, established that the grid produced nearly isotropic turbulence, that the length scale increased linearly with distance d from the grid,

$$l_t = \beta d, \tag{3}$$

where β is an empirically determined constant, and that the turbulent velocity decreased with distance, $u_t \sim d^{-1}$. The turbulent velocities were dependent on the grid geometry, given by M, the mesh spacing between the bars, and the grid motion, characterized by the oscillation frequency ω and amplitude A. Velocity u_t was found to be given by

$$u_t = C \frac{A^{\alpha} M^{2-\alpha} \omega}{d}, \tag{4}$$

where C and $\alpha \leqslant 2$ were empirically determined constants.

When turbulence occurs in stably stratified fluids, buoyancy forces tend to inhibit vertical motion. The Ozmidov (1965) length scale, L_O, arises from the balance of buoyancy and inertial effects,

$$L_O = \left(\frac{\varepsilon}{N^3} \right)^{1/2}, \tag{5}$$

with the dissipation rate of turbulent kinetic energy ε is given by

$$\varepsilon = \frac{{u_t}^3}{l_t}. \tag{6}$$

Stratification has little effect on turbulence with length scales $l_t < L_O$. However, as l_t approaches L_O buoyancy suppresses turbulence and overturning eddies reach their maximum vertical scale (i.e. $l_t \sim L_O$). This limit corresponds to an internal turbulent Froude number,

$$Fr_t \equiv \frac{u_t}{N l_t}, \tag{7}$$

of order one.

In grid-generated turbulence the Froude number decreases with distance from the grid. At a critical distance, d_N, $Fr_t \sim 1$. From (3), (4), and (7), this distance is

$$d_N \sim \left(\frac{CA^{\alpha}M^{2-\alpha}\omega}{\beta N}\right)^{1/2}. \tag{8}$$

More generally,

$$d_N \sim K_1\left(\frac{\omega}{N}\right)^{1/2}, \tag{9}$$

where the constant K_1 is a function of the grid characteristics and has the dimension of length.

A number of laboratory studies have demonstrated that the inhibition of vertical turbulent overturning by stratification occurs at the critical distance d_N from the grid. In experiments using mechanisms similar to the Hopfinger–Toly grid, Linden (1973), Turner (1973, 1986), Fernando (1988), and Fleury *et al.* (1991) examined uniform mixing over a horizontal plane. The initially rapid formation of a mixed layer was followed by the development of a sharp density interface and a reduced rate of vertical entrainment. The suppression of turbulent growth occurred at a height scale proportional to $(\omega/N)^{1/2}$.

In experiments where the imposed turbulence was spatially inhomogeneous, the effects of buoyancy not only arrested the vertical overturning, but also led to the simultaneous collapse of three-dimensional turbulence into lateral intrusions of mixed fluid. Maxworthy & Monismith (1988) and De Silva & Fernando (1998) used horizontal grids mounted in one section of a long rectangular tank to create a single layer of mixed fluid. Ivey & Corcos (1982), Thorpe (1982), and Browand & Hopfinger (1985) used vertically oriented planar grids to generate a 'wall' of turbulence. In these last experiments multiple horizontal layers of mixed but non-turbulent fluid intruded into the interior. The motion changed from three-dimensional turbulence to laminar intrusions at a distance from the grid again proportional to d_N (i.e. $(\omega/N)^{1/2}$), and the heights of the individual intrusions were consistent with the turbulent length scale $l_t|_{d_N}$ predicted from (3) at the critical distance.

Laboratory studies also demonstrated that rotation imposes similar constraints on three-dimensional turbulence. The analogy with stratified flow suggests that turbulent motions sufficiently close to an oscillating grid will behave independently of rotation. At a critical distance from the grid, rotation will suppress the vertical turbulent motion. This transition is expected when the turbulent Rossby number,

$$Ro_t \equiv \frac{u_t}{fl_t}, \tag{10}$$

approaches unity from above. For low Rossby numbers the flow becomes strongly two-dimensional and geostrophic. The properties of grid-generated turbulence, $u_t \sim d^{-1}$ and $l_t \sim d$, predict a critical distance for $Ro_t = O(1)$,

$$d_f \sim K_2\left(\frac{\omega}{f}\right)^{1/2}, \tag{11}$$

where K_2 is another grid-specific constant.

Dickinson & Long (1983) and Hopfinger, Browand & Gagne (1982) examined rotational inhibition of turbulence using vertically oscillating horizontal grids to generate horizontal planes of turbulent motion. At a distance proportional to $(\omega/f)^{1/2}$ the flow changed from three-dimensional turbulence to two-dimensional rotationally

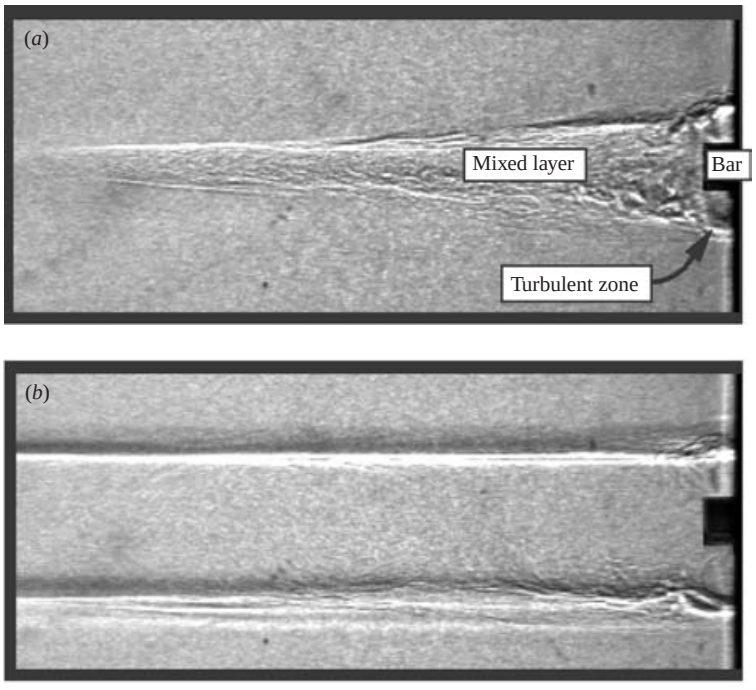

FIGURE 2. Side-view shadowgraphs of the turbulent zone and mixed layer in an experiment with $N = 66\,\mathrm{s}^{-1}$, $A = 0.35\,\mathrm{cm}$, and $\omega = 14\,\mathrm{s}^{-1}$. (*a*) Turbulent overturning and emergence of mixed layer at $t = 75\,\mathrm{s}$. (*b*) Mixed layer at $t = 3105\,\mathrm{s}$.

dominated flows with strong vertical coherence. Dickinson & Long observed a transition to organized vertically oriented sheets of dye, resembling Taylor curtains. Hopfinger *et al.* described the emergence of concentrated vortices with axes parallel to the axis of rotation. The horizontal scale of the vortices corresponded to the local integral length scale at the critical distance, $l_t|_{d_f}$, and so were proportional to $(\omega/f)^{1/2}$.

3.2. *Parameterization of the single-bar-induced turbulence*

As a prelude to the rotating experiments the turbulence produced by a single vertically oscillating bar was investigated in a series of non-rotating experiments carried out in a small tank. The 30.5 cm bar and plate assembly was mounted at one end of a 40 cm wide by 60 cm long rectangular tank. The tank was filled with linearly stratified salt water to a depth of 26 cm and covered with a rigid styrofoam lid. Five experiments with $N = [0.51, 0.54, 0.66, 0.34, 0.62]\,\mathrm{s}^{-1}$ were conducted. The turbulence and mixed-layer development were visualized with side-view shadowgraphs.

The shadowgraphs show the development of both the turbulent zone and a single mixed-layer intrusion which propagated into the tank interior. These features are illustrated in figure 2 with images from the experiment with $N = 0.66\,\mathrm{s}^{-1}$. Figure 2(*a*), at $t = 75\,\mathrm{s}$ after the initiation of bar motion, shows small-scale density features in front of the bar and distinct eddies above and below the bar. The turbulent zone has already grown to the height that it will maintain despite the lateral export of non-turbulent mixed fluid. Figure 2(*b*) shows an image at $t = 3105\,\mathrm{s}$, after the intrusion of mixed fluid has crossed the tank and returned to the bar. At this point mixed fluid fills the entire horizontal plane at the level of the bar and the turbulent zone resumes

growing vertically. The mixed layer thickens uniformly over time and the bounding high-gradient interfaces sharpen.

In general, the turbulent zone and the single intrusion are similar to the intrusions generated by the horizontally planar grids of Maxworthy & Monismith (1988) and De Silva & Fernando (1998). The experiments also show that the height of the turbulent zone grows approximately as $t^{1/8}$ for $Nt \geqslant 500$. This $t^{1/8}$ growth is consistent with previous experiments and scalings for layer growth (see § 6.2).

A quantitative parameterization of bar-induced turbulence was developed following the approach taken by Thorpe (1982). Thorpe used the Hopfinger–Toly model for l_t (3) and u_t (4) to construct expressions for the critical distance d_N (8) and for the turbulent length scale l_t at d_N. At the time when the layers first appeared, Thorpe recorded the distance of the turbulent front from the grid and the height of the intrusion. He assumed that the front location represented d_N and the layer heights approximated $l_t|_{d_N}$. Thorpe set the model exponent to the Hopfinger–Toly value, $\alpha = 1.5$, and solved for the constants of proportionality C and β in (3) and (8). He also examined the Ivey & Corcos (1982) data and determined values of C and β for the solid-plate multibar grid used in their experiments.

Here it is assumed that the turbulent length scales for the single bar mechanism are similar to those of the Ivey & Corcos grid that had horizontally oriented bars with a $1.27 \times 1.27\,\mathrm{cm}^2$ cross-section. The value Thorpe found for the Ivey & Corcos grid, $\beta = 0.24$, is used in the parameterization of l_t (3) and the formula for d_N (8). Since neither bar size nor amplitude are varied, the parameterization of turbulent velocity u_t (4) is written solely in terms of grid frequency ω and distance from the bar d,

$$u_t = G\frac{\omega}{d}, \tag{12}$$

where G replaces $CA^{\alpha}M^{2-\alpha}$ and has the dimensions of length squared. Observations of the layer height at the transition from turbulent overturning to laminar intrusion were used in the experiment with $N = 0.66\,\mathrm{s}^{-1}$ to evaluate d_N and solve for the constant, giving $G = 0.23\,\mathrm{cm}^2$. Thus the critical distance and associated turbulent length scale were given by $d_N = 1.9(\omega/N)^{1/2}\,\mathrm{cm}$ and $l_t|_{d_N} = 0.45(\omega/N)^{1/2}\,\mathrm{cm}$, respectively. The measurement techniques and calculations are presented in detail in Wells (2003).

The formulae for d_N and $l_t|_{d_N}$ were applied to the remaining non-rotating experiments with $N = [0.51, 0.54, 0.34, 0.62]\,\mathrm{s}^{-1}$. Observations matched predicted values to within 20%. The greatest mismatch occurred in the one experiment that was visualized using dye in the mixed layer. Otherwise the shadowgraph image data were within 2% to 9% of the predicted values. While turbulent velocities and length scales were not directly measured in the experiments, the inferred values for the constants, β and G, yielded plausible and consistent predictions for the mixed-layer height.

A quantity of interest in the derivation of length scales for the rotating mixing experiments is the inverse of the turbulent timescale $(l_t/u_t)^{-1}$. From (3) and (12) it can be written as

$$\frac{u_t}{l_t} = \gamma^2\frac{\omega}{d^2}. \tag{13}$$

Here $\gamma \equiv (G/\beta)^{1/2} = 0.98\,\mathrm{cm}$ using G and β determined above.

3.3. *Experimental length scales*

The length scales used in evaluating the rotating experiments described in the following sections include the width of the mixing region, given by the bar width L_B, and three other scales constructed from the frequencies N, f and ω. Two follow from

the assumption that motion at the interface of the turbulent zone and the ambient rotating stratified fluid is set by a balance between the intrinsic time scale of the turbulence, l_t/u_t, and the buoyancy and rotation periods, N^{-1} and f^{-1}. The distances from the bar at which the turbulent Froude (7) and Rossby (10) numbers equal unity can be found using the bar parameterization (13). These are then identified with a buoyancy height scale, H_N,

$$H_N \equiv \gamma \left(\frac{\omega}{N}\right)^{1/2} \text{(cm)}. \tag{14}$$

and a rotational length scale, L_f,

$$L_f \equiv \gamma \left(\frac{\omega}{f}\right)^{1/2} \text{(cm)}. \tag{15}$$

The third length scale used in analysing the experimental results is the internal Rossby radius of deformation, hereafter referred to as the deformation radius, based on a vertical height h ($\sim H_N$),

$$L_R = \frac{Nh}{f}. \tag{16}$$

The deformation radius is the horizontal scale at which rotation begins to control the outflow.

The experimental variations in N, f, and ω listed earlier give $4 \leqslant H_N \leqslant 9$ cm, $3 \leqslant L_f \leqslant 7$ cm and $1.6 \leqslant L_R \leqslant 12$ cm.

4. Qualitative results

4.1. *Export of mixed fluid from the turbulent zone*

Turbulent mixing of a rotating, stratified fluid begins with the onset of the bar oscillation at $t = 0$. The typical development of the mixed layer is seen in images from an experiment with $(N, f) = (0.9, 0.9)\,\text{s}^{-1}$ (figure 3). Note that the experiments shown in figures 3 to 5 all have $\omega = 14\,\text{s}^{-1}$ and $L_B = 20.3$ cm. Within the first 30 s a dyed turbulent region has formed around the bar and mixed fluid has collapsed into an outwardly moving intrusion (figure 3*a*). At $t = 60$ s (figure 3*b*), the turbulent region at the bar has reached its full height (thickness) and the emergent mixed layer is well-defined. Figures 3(*c*) and 3(*d*) show that the layer height remains essentially uniform as mixed fluid advances into the interior ($t = 300$ and 600 s).

Images from experiments with $\frac{1}{3} \leqslant N/f \leqslant 3$ indicate that vertical mixing is restricted by stratification, while the lateral distribution of mixed fluid depends on both N and f. Figure 4 shows mixed layers at $t = 360$ s from four experiments with different values of the buoyancy and Coriolis frequencies. Compare figures 4(*a*) and 4(*b*) where $N = 0.3\,\text{s}^{-1}$, and $f = 0.3$ and $0.9\,\text{s}^{-1}$, respectively, with figures 4(*c*) and 4(*d*) where $N = 0.9\,\text{s}^{-1}$ and $f = 0.3$ and $0.9\,\text{s}^{-1}$. The layer heights decrease with increasing stratification and are independent of f. However, the length of the intrusion is affected by both $N$and f. Greater length is associated with higher buoyancy frequencies and lower Coriolis frequencies.

Figure 5 presents top view images of the experiments in figure 4 with $N/f = 3$ (figure 5*a*, *b*, *c*) and $N/f = \frac{1}{3}$ (figure 5*d*, *e*, *f*). When $N/f = 3$ the emerging fluid moves directly across the tank (see figures 5*a* and 5*b* at $t = 360$ s and $t = 900$ s, respectively). The dyed layer encounters the opposite wall at $t = 1200$ s and by $t = 3600$ s (figure 5*c*)

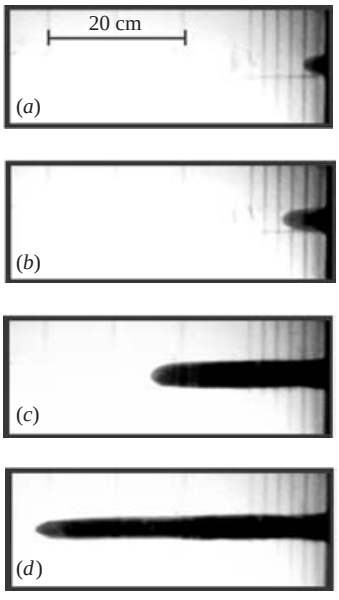

FIGURE 3. Dye images for an experiment with $(\omega, N, f) = (14, 0.9, 0.9)\,\mathrm{s}^{-1}$ and $L_B = 20.3\,\mathrm{cm}$. Side view of mixed layer. (*a*) $t = 30\,\mathrm{s}$, (*b*) $t = 60\,\mathrm{s}$, (*c*) $t = 300\,\mathrm{s}$, (*d*) $t = 600\,\mathrm{s}$.

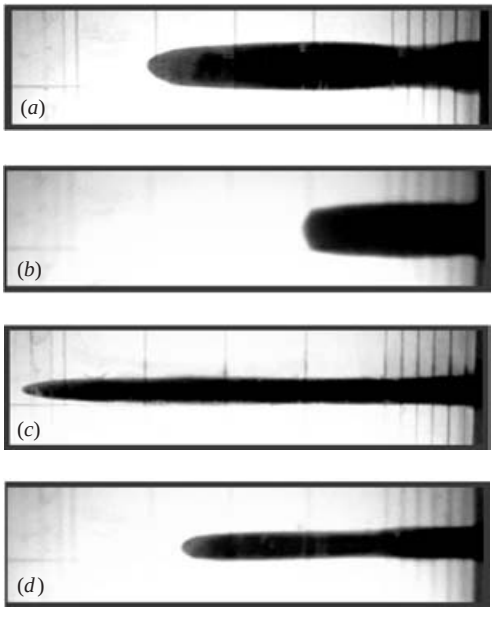

FIGURE 4. Side view dye images for four experiments with $\omega = 14\,\mathrm{s}^{-1}$ and $L_B = 20.3\,\mathrm{cm}$ at $t = 360\,\mathrm{s}$. (*a*) $N/f = 1$, $(N, f) = (0.3, 0.3)\,\mathrm{s}^{-1}$. (*b*) $N/f = 1/3$, $(N, f) = (0.3, 0.9)\,\mathrm{s}^{-1}$. (*c*) $N/f = 3$, $(N, f) = (0.9, 0.3)\,\mathrm{s}^{-1}$. (*d*) $N/f = 1$, $(N, f) = (0.9, 0.9)\,\mathrm{s}^{-1}$.

it has spread over the entire tank interior. For $N/f = \frac{1}{3}$ the front of mixed fluid never crosses the tank. At $t = 360\,\mathrm{s}$ (figure 5*d*) the flow has gone less than one half the distance covered in the same time period by the flow in figure 5(*a*). By $t = 900\,\mathrm{s}$ (figure 5*e*) a field of eddies has formed and the cross-tank progress of the coherent

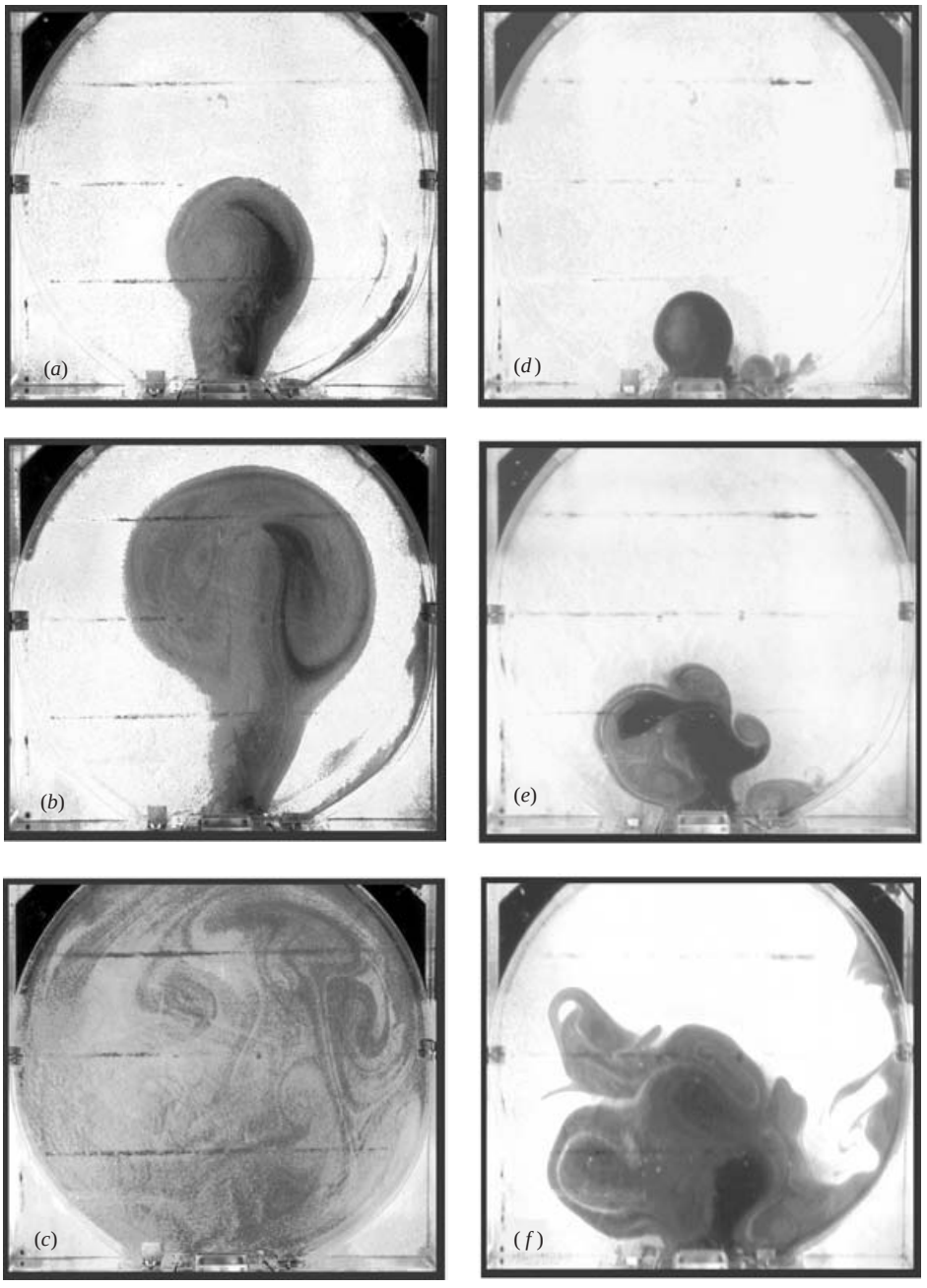

FIGURE 5. Dye images. (a, b, c) Experiment with $N/f = 3$, $(\omega, N, f) = (14, 0.9, 0.3)\,\mathrm{s}^{-1}$. (d, e, f) Experiment with $N/f = 1/3$, $(\omega, N, f) = (14, 0.3, 0.9)\,\mathrm{s}^{-1}$. $L_B = 20.3\,\mathrm{cm}$. From top to bottom $t = 360\,\mathrm{s}$, $t = 900\,\mathrm{s}$, $t = 3600\,\mathrm{s}$.

front has been arrested. At $t = 3600\,\mathrm{s}$ (figure 5f) the eddies have grown and dispersed, but the mixed fluid is still confined near the bar. For both examples in figure 5 weak boundary currents are present; however, at most 5% and 1% of the mixed-fluid volume flux is carried by these currents for $N/f = 3$ and $\frac{1}{3}$, respectively.

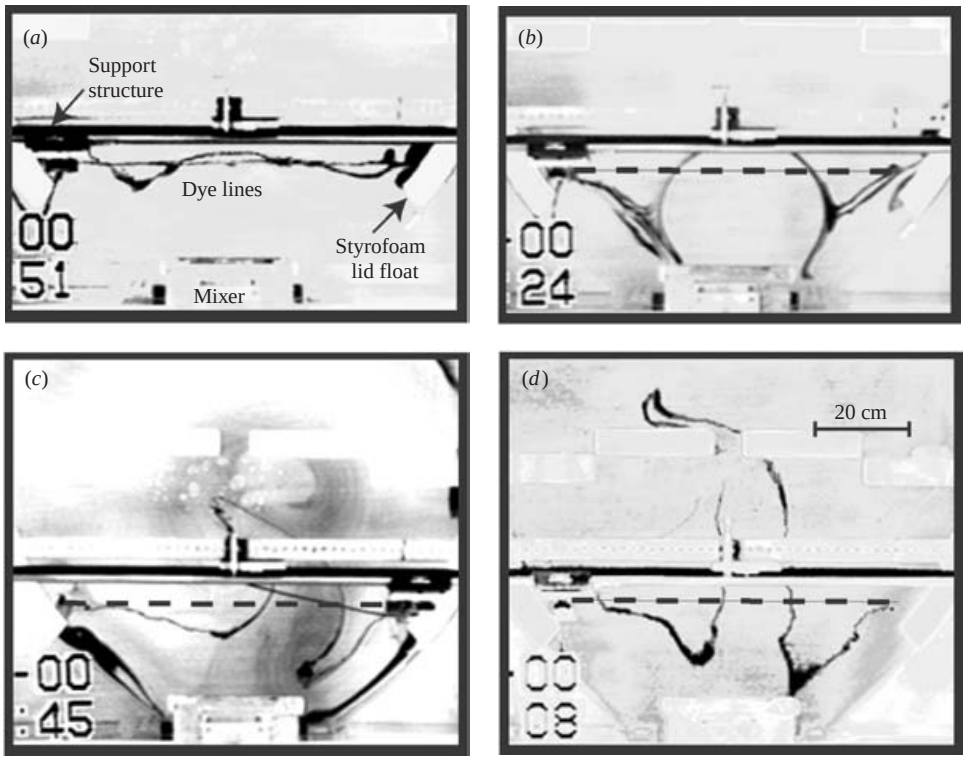

FIGURE 6. Dye line images for experiment with $N/f = 1$, $(\omega, N, f) = (14, 0.7, 0.7)\,\mathrm{s}^{-1}$ and $L_B = 30.5\,\mathrm{cm}$. The dashed lines indicate the original position of the dye lines. Images taken at times (*a*) $t = 420\,\mathrm{s}$, (*b*) $t = 600\,\mathrm{s}$, (*c*) $t = 1380\,\mathrm{s}$, (*d*) $t = 25\,200\,\mathrm{s}$.

All the localized vertical boundary mixing experiments show a similar pattern. Mixed fluid is exported directly out into the tank, with little or no fluid exported in a boundary current. The absence of dye at the sides of the mixing region suggests that horizontal entrainment of ambient fluid at the level of the mixing bar may be occurring.

4.2. *Entrainment into the turbulent zone*

Circulation of ambient fluid outside the dyed layer is investigated through two flow visualization techniques. Potassium permanganate crystals are dropped at selected locations to create full-depth vertical dye streaks that give the vertical structure of the flow, and horizontal streaks of neutrally buoyant dye are laid down at specified depths to illustrate the plan-view structure. Experiments are done for $N/f = [\frac{1}{4}, \frac{1}{2}, 1, 2]$. The experiment with $N/f = 1$, shown in figure 6, typifies the plan-view observations for dye lines at the approximate depth of the mixing bar. The images show top views of the tank with selected features labelled in figure 6(*a*). The dashed lines in figures 6(*b*, *c*, *d*) give the initial positions of dye streaks.

Figure 6(*a*) at $t = 7\,\mathrm{min}$ shows two dye lines. One, laid down at $t = 300\,\mathrm{s}$, has not moved significantly. The other, laid down at $t < 0$, has been displaced outwards at the centre and in toward the mixing bar at the sides. The outlined areas have a 1.67 ratio of inward to outward flow. The uneven flow ratio may indicate that fluid is entrained vertically as well as horizontally when mixing is initiated. By $t = 600\,\mathrm{s}$, both lines have been drawn into the the sides of the mixing region and a central outward flow

is clearly established (figure 6*b*). Later dye line displacements show an approximate horizontal mass balance at the level of the mixing. The inbound and outbound areas in figures 6(*c*) and 6(*d*) ($t = 1380$ s and 25 200 s, respectively) exhibit 1:1 ratios. Horizontal dye lines at 5 cm above and below the bar depth give similar flows, but with much smaller velocities, suggesting that the circulation at the level of the mixed layer indicates the general pattern. More information on the vertical structure of the velocity field comes from the vertical dye traces left by potassium permanganate crystals. Dye columns are placed directly in front, and through, the lateral intrusion of mixed fluid. Vertical streaks are also placed to the side of the exported fluid, in the regions where the plan-view images indicated flow towards the mixing zone. The displacement of dye traces in advance of the intrusion shows little or no coherent motion, while the profiles through the mixed layer show a unidirectional velocity over the whole depth of the fluid column. The velocity reaches its maximum at the mixed-layer level and drops off rapidly above and below it, in agreement with the pattern inferred from the horizontal dye lines. Profiles in undyed areas close to the grid show horizontal flow of ambient fluid towards the mixing bar. Fluid at the level of the mixed layer is drawn into the sides of the turbulent zone.

These observations imply that, except for the very early stages, the production of mixed fluid relies on horizontal, rather than vertical, entrainment. The observations support a picture of a mixing region of finite vertical and horizontal dimension that draws stratified ambient fluid in along the walls of the tank at the level of the bar and exports mixed fluid directly into the interior.

5. Quantitative analysis and scaling

Measurements of the mixed-fluid outflow cover the period between the emergence of the mixed layer and the appearance of disturbances on the advancing front. Measured quantities include mixed-layer height, intrusion advancement, and the plan-view area and volume of mixed fluid.

The first fourteen experiments are conducted with a single bar size, $L_B = 30.5$ cm. Variations in L_B are addressed in § 7. Eight experiments include both rotation and stratification. Two experiments are run with $\omega = [7, 28]\ \mathrm{s}^{-1}$. In all other cases, $\omega = 14\ \mathrm{s}^{-1}$. In addition, three experiments have stratification but no rotation, and three have rotation only. Table 1 lists the variables for all experiments, including those in § 7 with $L_B = [15.2, 20.3, 22.9]$ cm.

5.1. *Data sources*

The main sources of quantitative data are the conductivity probe records and the images of the dyed fluid. The probe measurements provide a detailed look at the evolution of the vertical density structure. Figure 7 shows a series from Experiment 6 of density vs depth profiles taken 18.7 cm in front of the bar. The profile at $t = 300$ s shows the initial linear density distribution as the mixed fluid has not yet reached the probe. At $t = 900$ s a step in the linear density profile marks the arrival of the intrusion. By $t = 1800$ s the step height is well-established. The dotted lines show five additional profiles taken between $t = 2700$ s and $t = 14\,880$ s. The intrusion is characterized by a well-mixed middle zone bounded by two zones of high density gradient. In the period after $t = 1800$ s, the mixed zone grows from 2.8 to 3.9 cm, while the overall vertical extent of the intrusion remains relatively constant. The intrusion height is defined as the height of both the mixed middle boundary and the high-gradient boundary. It is measured by the intersection points of the ambient, approximately linear, density

Experiment	L_B (cm)	ω (s^{-1})	N (s^{-1})	f (s^{-1})	N/f	h_m (cm)
1	30.5	14	0.33	0.35	0.94	6.33
2	30.5	14	0.75	0.35	2.14	4.45
3	30.5	14	0.36	0.7	0.51	5.93
4	30.5	14	0.69	0.7	0.99	4.32
5	30.5	14	0.36	1.4	0.26	6.39
6	30.5	14	0.69	1.4	0.49	4.46
7	30.5	7	0.63	0.7	0.9	3.58
8	30.5	28	0.61	0.7	0.87	5.91
9	30.5	14	0.21	0	–	7.96
10	30.5	14	0.35	0	–	5.99
11	30.5	14	0.69	0	–	4.33
12	30.5	14	0	0.35	–	–
13	30.5	14	0	0.7	–	–
14	30.5	14	0	1.4	–	–
15	15.2	14	0	0.35	–	–
16	15.2	14	0.67	0.35	1.91	4.36
17	15.2	14	0.66	0.7	0.94	4.36
18	15.2	14	0.66	1.4	0.47	4.44
19	20.3	14	0.83	0.3	2.77	3.83
20	20.3	14	0.32	0.3	1.07	6.17
21	20.3	14	0.33	0.88	0.38	6.17
22	22.9	14	0.65	0.35	1.86	4.34
23	22.9	14	0.67	0.7	0.96	4.26
24	22.9	14	0.67	1.4	0.48	4.42
25	15.2	14	0.67	0	–	4.68
26	20.3	14	0.85	0	–	3.89
27	22.9	14	0.67	0	–	4.53

TABLE 1. Summary of the independent variables for each experiment: bar width L_B, bar frequency ω, buoyancy frequency N and Coriolis frequency f. Also listed are N/f and the measured mixed layer height h_m.

curve with the tangents of the high-gradient slopes. The probe data give an average intrusion height, $h_p = (4.5 \pm 0.2)$ cm. A second step, seen at the bottom of the density profiles in figure 7, is due to mixing by the base of the grid support plate. In later experiments the edge of the plate has been chamfered and the secondary step is greatly reduced.

The probe measurements at two locations, one 18.7 cm in front of the grid and the other 93.3 cm across the tank, register density changes only after the arrival of dyed fluid. The appearance of dye is therefore associated with the presence of mixed fluid. A comparison of layer thickness from the video images of dye to that determined from the conductivity probe profiles shows a consistent relationship between the two methods of measurements.

The dye distributions seen in figures 3 and 4 show one well-defined layer. Within the first 100 s of bar motion, the dyed layer thickens and reaches a height that remains nearly steady over the duration of the experiments and nearly uniform over the length of the intrusion. Layer height measurements based on digitized video images are taken about 2 cm in front of the bar where the images are sharpest. Mean values for the dyed layer heights, h_m, in each experiment are calculated from data collected for $t > 100$ s. Corresponding mean values from the probe profiles, h_p, are calculated from data collected after the nose of the intrusion has passed the profiling site. The

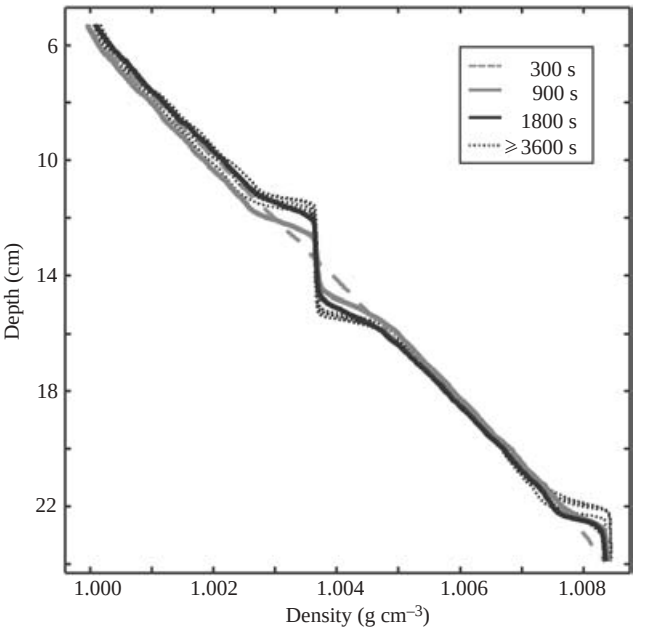

FIGURE 7. Eight density profiles for experiment 6 with $(\omega, N, f) = (14, 0.69, 1.40)\,\mathrm{s}^{-1}$ and $L_B = 30.5\,\mathrm{cm}$, taken 18.7 cm in front of the mixing bar between $t = 300\,\mathrm{s}$ and $t = 14880\,\mathrm{s}$.

dyed layer in Experiment 6 has a mean height of $h_m = (4.5 \pm 0.1)\,\mathrm{cm}$, comparing well with the 4.5 cm from the probe measurement.

A straight line fit of the dyed layer heights to the probe profile heights for all the stratified, rotating experiments, gives

$$h_m = (1.00 \pm 0.07) h_p, \tag{17}$$

therefore allowing the numerous video images to give good estimates of the intrusion thickness. Even though the dye does not measure the thoroughness of the mixing, it serves as a marker for flows of mixed fluid from the turbulent zone. In the following subsections digitized video images of the dye are used to document and quantify the evolution of mixed fluid.

5.2. *Vertical mixing and layer height*

Mixed layer height h_m, based on a time mean of the dye images, scales well with the buoyancy scale height, $H_N = \gamma(\omega/N)^{1/2}$ (14), as shown in figure 8. Recall the constant $\gamma = 0.98\,\mathrm{cm}$. The errorbar on selected data points gives the standard deviation about the mean height for the individual experiment. On average, the standard deviation is 5% of the mean value. A linear fit to the data gives

$$h_m = (0.97 \pm 0.05)\gamma \left(\frac{\omega}{N}\right)^{1/2}. \tag{18}$$

This dependence of layer height on $\gamma(\omega/N)^{1/2}$ is consistent with the earlier non-rotating studies of Ivey & Corcos (1982), Thorpe (1982), and Browand & Hopfinger (1985).

The data in figure 8 are from Experiments 1–11, both with and without rotation, and show no dependence on f. Davies *et al.* (1991) did find a dependence of layer height on rotation, but only after mixed fluid had circled the tank and returned to

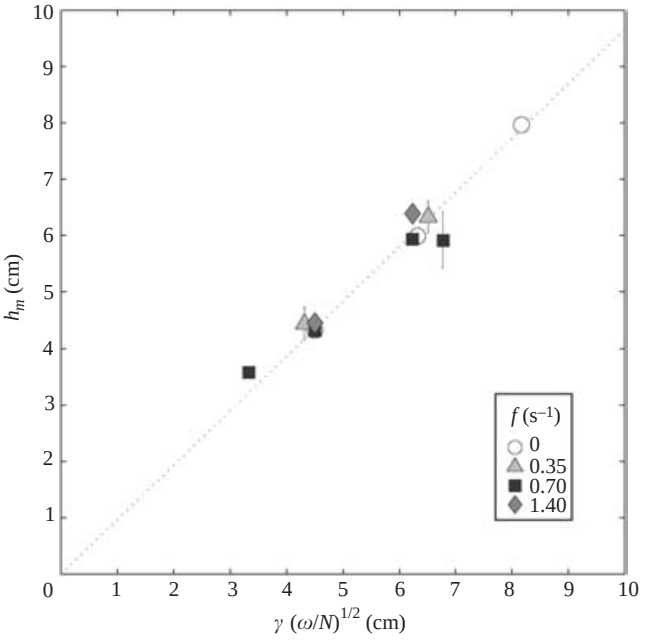

FIGURE 8. Mean height of mixed layer versus buoyancy scale height (14), for experiments with $7 \leqslant \omega \leqslant 28\,\mathrm{s}^{-1}$, $0.33 \leqslant N \leqslant 0.75\,\mathrm{s}^{-1}$, $0 \leqslant f \leqslant 1.40\,\mathrm{s}^{-1}$, and $L_B = 30.5\,\mathrm{cm}$. Symbols indicate rotation rates for individual experiments.

the source region. The short-term mixed-layer height was unaffected by rotation and also scaled with $(\omega/N)^{1/2}$.

5.3. *Advance of the mixed-layer front*

The horizontal distribution of the mixed fluid in the rotating stratified experiments is investigated by determining the position of the mixed-layer front along an axis normal to the bar and the total plan view area of dye (i.e. mixed fluid). The advance of the mixed-layer front versus time is shown in figure 9. The intrusion length l_m is determined from the side-view images. Time is normalized by f^{-1} and the length l_m by the deformation radius, $L_R = Nh/f$ (16), with h given by h_m (18). The data collapse to an intrusion length that grows approximately as $t^{2/3}$,

$$l_m = (0.20 \pm 0.04)\, L_R (ft)^{0.65 \pm 0.04}. \tag{19}$$

The speed of the front is proportional to Nh_m, the speed of a gravity current with height h_m, with a weak dependence on non-dimensional time ft,

$$\frac{\mathrm{d}l_m}{\mathrm{d}t} = 0.13\, Nh_m (ft)^{-0.35}. \tag{20}$$

The time dependence may be due to the two-dimensional spreading of the front which is certainly affected by rotation.

The measurements of intrusion length are taken until the outflow front becomes irregular and develops baroclinic eddies. This occurs when

$$l_m = (10.3 \pm 1.7) L_R \tag{21}$$

as shown in figure 10. The first disturbances appear in the emergence of tendrils of dyed fluid or the formation of multiple lobes. In figure 5(a, b, c) $L_R = 11\,\mathrm{cm}$ and the

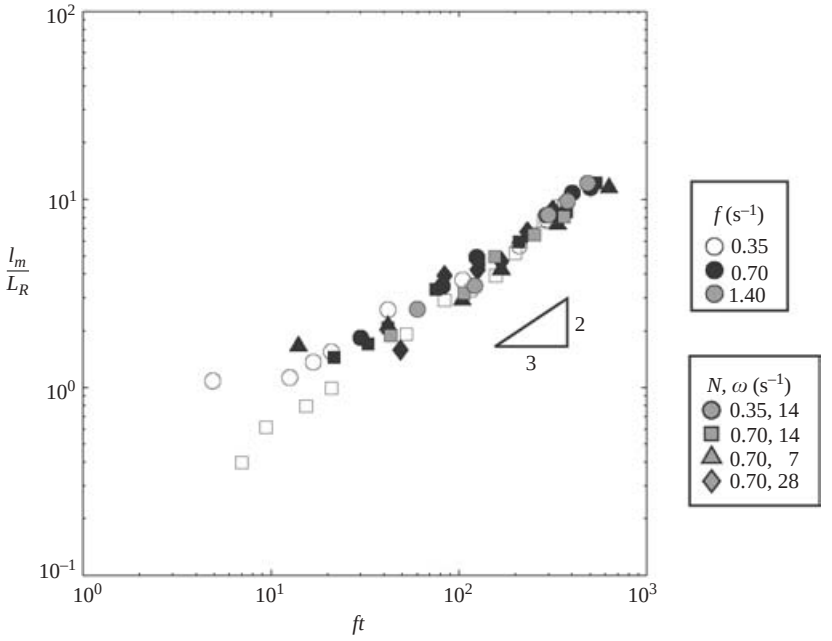

FIGURE 9. Advance of the mixed fluid along the normal axis. Intrusion length normalized by the deformation radius, $L_R = (N/f)h_m$, versus non-dimensional time ft, for all rotating stratified experiments with $L_B = 30.5$ cm.

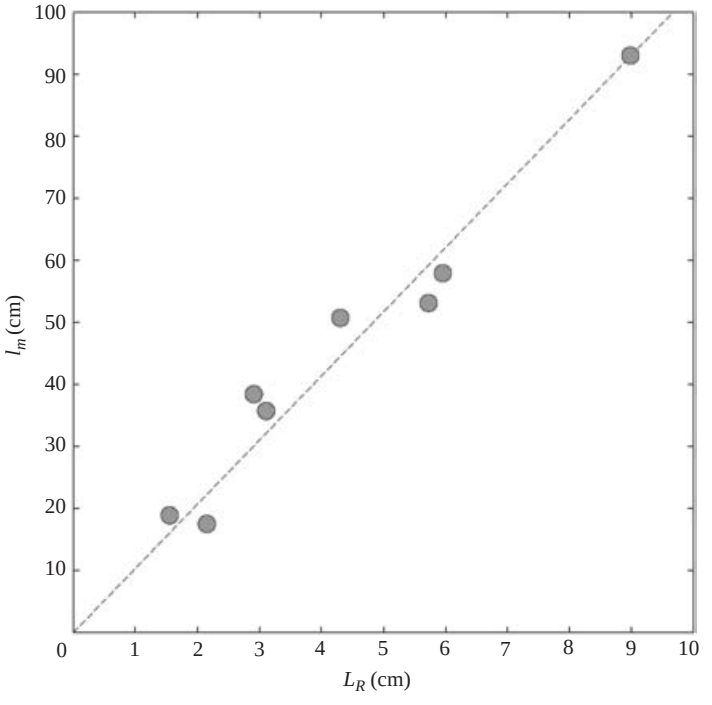

FIGURE 10. Position of the mixed fluid along the normal axis at the onset of instability. Length of intrusion versus deformation radius, $L_R = (N/f)h_m$, for all rotating stratified experiments with $L_B = 30.5$ cm.

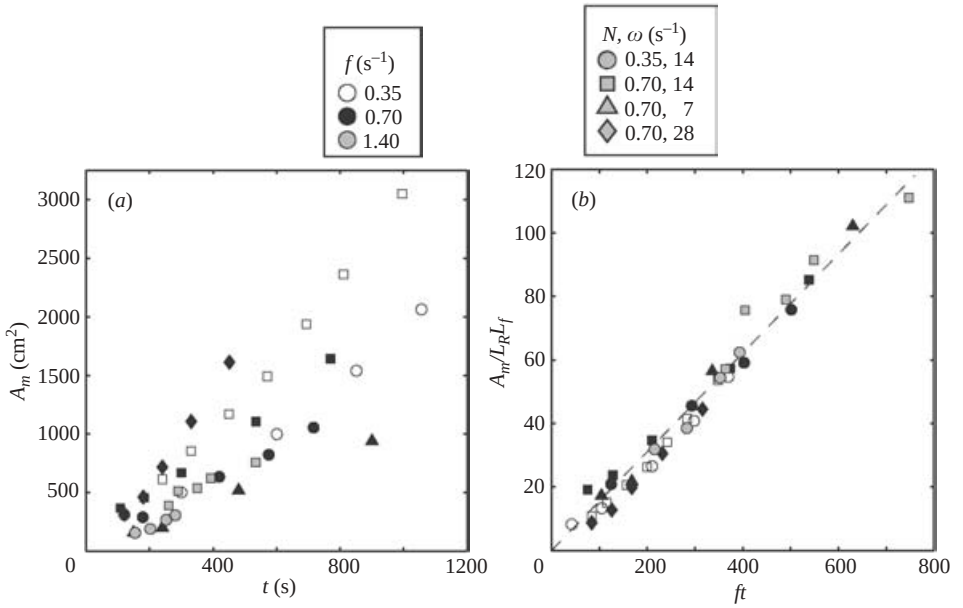

FIGURE 11. Horizontal area of mixed fluid for all rotating stratified experiments with $L_B = 30.5$ cm. Symbols indicate values of ω, N and f. (*a*) Area (cm^2) vs time (s). (*b*) Area normalized by $L_R L_f$, given by (16) and (15), vs non-dimensional time ft.

intrusion crosses the tank inner diameter of 112 cm without developing instabilities. In figure 5(*d*, *e*, *f*) $L_R = 2.1$ cm. At $t = 360$ s the intrusion length is $\sim 10 L_R$. Beyond this point it develops multiple lobes, as shown in figure 5(*e*), and the continued outflow of mixed fluid, shown in figure 5(*f*), involves a complex eddy field that transports mixed fluid further into the tank interior.

5.4. *Lateral spreading and volume flux of the mixed layer*

Prior to the development of instabilities the advancing front exhibits a simple geometry from which the plan-view area of mixed fluid, A_m, can easily be determined. The dimensional measurements of area vs time are shown in figure 11(*a*). One obvious scaling of the data is to normalize the area with L_R^2 and time with f^{-1}. However, this does not collapse the data very well. A better fit is found when the area is scaled by $L_R L_f$. The scaled area data, shown in figure 11(*b*), now collapse to a straight line with a correlation coefficient $r = 0.99$,

$$A_m = (0.15 \pm 0.03) L_R L_f ft. \tag{22}$$

Scaling the area by $L_R L_f$ suggests that the horizontal spreading of mixed fluid is more than an adjustment of laminar outflow to background rotation. It implies that the characteristics of the mixed layer are determined, in part, by the rotational control of turbulent motion.

Rotational control of bar-generated turbulence occurs when the turbulent Rossby number (10) drops to $O(1)$ or below and the turbulence becomes essentially two-dimensional and columnar as in the experiments of Hopfinger *et al.* (1982) and Dickinson & Long (1983). Rotational influence in the absence of stratification is examined in Experiments 12–14. While the dye injected at the bar does not capture the transition from isotropic turbulence to rotationally dominated flow, it does show

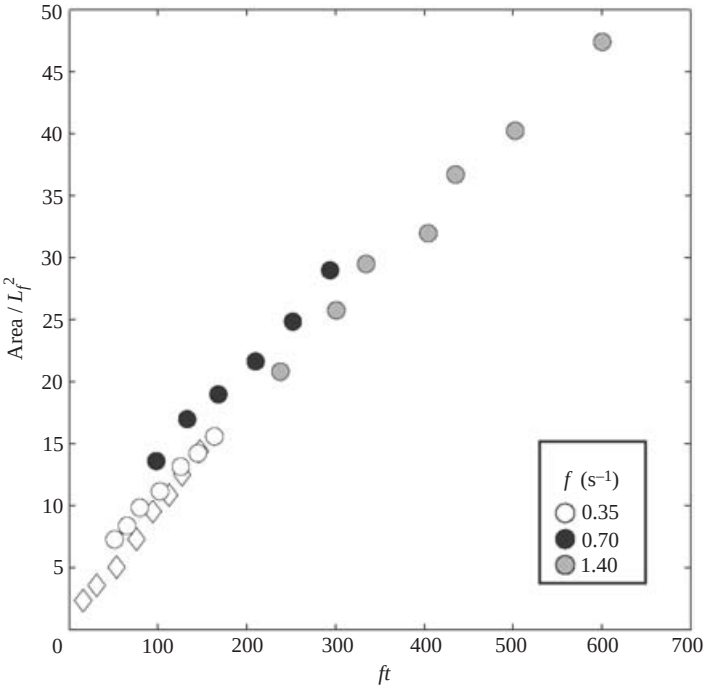

FIGURE 12. Horizontal area of dyed fluid for unstratified rotating experiments. Area normalized by the rotational length scale, L_f^2 (15), vs non-dimensional time ft. The circles indicate experiments with $L_B = 30.5\,\text{cm}$. The diamonds indicate an experiment with $L_B = 15.2\,\text{cm}$ (see § 7).

the large-scale Lagrangian advection of fluid away from the mixer. The dyed fluid quickly forms into vertical sheets which span the full depth and expand horizontally into the undisturbed interior. Figure 12 shows the growth of the plan-view area of dyed fluid. The relationship between the area A and the rotational length scale L_f collapses reasonably well with the scaling

$$A = (0.09 \pm 0.02) L_f^2 ft. \tag{23}$$

This result, although limited, indicates that the horizontal extent of motion in a homogeneous fluid is consistent with the idea of rotational inhibition of turbulence.

Returning to the stratified experiments, since mixed-layer height is approximately constant prior to the development of instabilities, the volume of mixed fluid in the stratified experiments is $V_m = h_m A_m$ (for $t > 150\,\text{s}$). From (22),

$$V_m = (0.16 \pm 0.03) L_R L_f h_m ft. \tag{24}$$

The slight change in the constant of proportionality is due to the difference between the measured mixed-layer heights and the scaling formula for h_m (18). The volume flux of mixed fluid is constant,

$$\frac{\mathrm{d}V_m}{\mathrm{d}t} = Q = 0.16 L_R L_f h_m f. \tag{25}$$

Interestingly, this scaling suggests that the volume flux is independent of the bar width L_B, though this has yet to be demonstrated as all the experiments considered

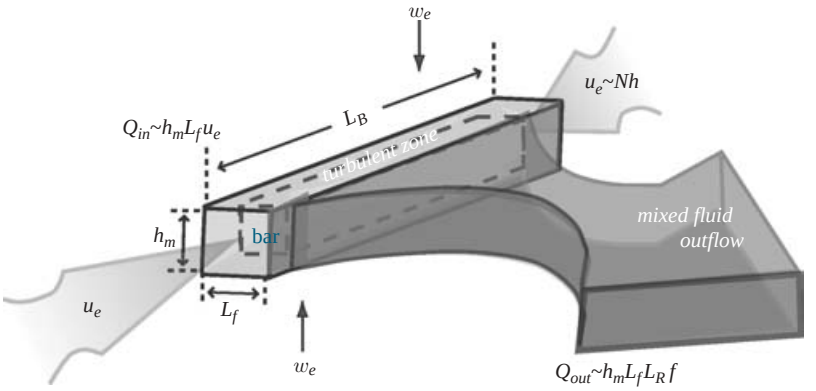

FIGURE 13. A schematic diagram showing the outward flux of mixed fluid, and the lateral entrainment of stratified fluid at the sides of the turbulent zone. The dimensions of the turbulent zone are labelled, $L_B \times L_f \times h_m$, where L_B is the bar width and L_f and h_m are given by (15) and (18), respectively.

have $L_B = 30.5$ cm. In the next section a simple physical scaling model is proposed to rationalize this result, and then is tested with additional experiments using variable L_B.

6. A model for mixing in the presence of rotation

6.1. *Model of lateral entrainment*

An entrainment model is proposed that provides a physical interpretation for the volume flux of exported mixed fluid. The basic features of the model are illustrated in figure 13. The assumptions of the model are as follows. The volume of the turbulent zone scales as $V_t \sim L_B L_f h_m$. Horizontal entrainment dominates any vertical entrainment. This assumption is discussed more fully below. Horizontal entrainment is at the sides of the mixing zone (figure 6), and occurs over the vertical scale h_m and the lateral scale L_f, perpendicular to the wall. The inflow is assumed to be in thermal wind balance. Scaling the depth-integrated thermal wind, $v \sim f^{-1}(g/\rho_o)(\Delta\rho/\Delta x)\Delta z$, with the deformation radius, $L_R = Nh_m/f$, for Δx, the mixed layer depth h_m for Δz, and the ambient stratification N gives the entrainment velocity, $u_e \sim Nh_m$.

As sketched in figure 13, ambient fluid enters across a surface area, $h_m L_f$, with the velocity u_e giving an influx

$$Q_{in} \sim h_m L_f u_e. \tag{26}$$

With negligible vertical entrainment, the mixed-fluid outflow must equal twice the inflow, thus with $u_e \sim Nh_m = L_R f$,

$$Q_{out} \sim h_m L_f L_R f. \tag{27}$$

Density is conserved since the inflow is linearly stratified and the outflow mixed with the mean density. The scaling is consistent with the experimental result (25), and is independent of the mixing zone width, L_B.

6.2. *Model of vertical entrainment*

An alternative hypothesis is that production of mixed fluid occurs through vertical entrainment only. The assumptions for this model are as follows. The volume of the turbulent zone is again $V_t \sim L_B L_f h_m$. Vertical entrainment of unmixed fluid occurs

across the upper and lower surfaces of the turbulent zone over the area $L_B L_f$. Horizontal entrainment is negligible.

The vertical inflow velocity is based on an entrainment law of the form $w_e/u_t \sim Ri_t^{-3/2}$, where the Richardson number $Ri_t \equiv N^2 l_t^2/u_t^2$. The rapid establishment of mixed-layer height h_m and the development of sharp density interfaces above and below the layer are consistent with earlier studies of non-rotating grid-generated turbulent entrainment which support the $Ri_t^{-3/2}$ dependence (Linden 1973; Turner 1973, 1986; Maxworthy & Monismith 1988; Fleury *et al.* 1991). The $t^{1/8}$ growth rate of the non-rotating small tank experiments reported in § 3.2 is also consistent with predictions of the Maxworthy–Monismith mixed-layer model.

Maxworthy & Monismith defined $w_e \equiv \mathrm{d}h/\mathrm{d}t$. Using the Denton & Wood (1981) formula for w_e as a function of $Ri_t^{-3/2}$ and the Hopfinger & Toly (1976) grid parameterization of turbulent properties, Maxworthy & Monismith showed that, for $Nt \gg 1$, the $Ri_t^{-3/2}$ power law gave $h \approx 1.15(K/N)^{1/2}(Nt)^{1/8}$, where $u_t = 0.29K/h$ and $(K/N)^{1/2}$ denotes the height of the mixed layer after a rapid adjustment phase. When the single-bar parameterizations of u_t and l_t (13) are used in the Maxworthy–Monismith calculation, $h \approx 1.11 h_m (Nt)^{1/8}$, implying that $w_e = 0.14 N h_m (Nt)^{-7/8}$, with h_m given by (18).

Fleury *et al.* (1991) studied vertical entrainment in rotating and non-rotating stratified fluids, and in the non-rotating case determined $w_e/u_t = 1.6 Ri^{-3/2}$. The Fleury *et al.* formula implies a vertical entrainment velocity for single-bar turbulence similar to that derived using the Denton & Wood relation,

$$w_e = 0.15 N h_m (Nt)^{-7/8}. \tag{28}$$

Fleury *et al.* demonstrated that rotation inhibited vertical entrainment for $N/f < 3$. Thus, for the present experiments, (28) provides an upper bound estimate of the vertical velocity w_e. The formula is applied for times $t > 100$ s, after the height h_m has been set. Vertical flux across the top and bottom surfaces is given by

$$Q_{vert} = 0.30 L_B L_f N h_m (Nt)^{-7/8}, \tag{29}$$

which by continuity is equal to the outflow of mixed fluid Q_{out}. Note that unlike the lateral entrainment model, the flux is proportional to the mixing-region width L_B.

The total volume of mixed fluid is calculated from the establishment of the mixed-layer height, at $t \approx 100$ s, to the typical upper limit of volume measurements at $t \approx 1000$ s. The parameters of Experiment 8 predict the maximum vertical entrainment,

$$V_{tot} = \int_{100\,\mathrm{s}}^{1000\,\mathrm{s}} Q_{vert}\,\mathrm{d}t = 1800\,\mathrm{cm}^3. \tag{30}$$

Experiment 4, with more typical parameters, results in $V_{tot} = 800$ cm^3. For these two examples, the observed changes in volume during the same period are 25 500 cm^3 and 9000 cm^3, respectively. Thus, the estimates of vertical entrainment account for only 7% and 9% of volume growth.

However, the assumption $w_e \sim t^{-7/8}$ may be incorrect and lead to an underestimate of the net vertical entrainment in the case of localized mixing. A modified model assumes a reduction in vertical entrainment with the establishment of mixed layer height h_m, but a constant entrainment rate thereafter. A rough estimate of volume

change is made by calculating the vertical flux (29) during the first 10 s after layer height has been established. The result is then multiplied by 90 to cover the entire 900 s period,

$$V_{tot} = 90 \int_{100\,\mathrm{s}}^{110\,\mathrm{s}} Q_{vert}\, \mathrm{d}t. \tag{31}$$

For the experiment with maximum flux $V_{tot} = 5600$ cm^3 and for the more typical experiment $V_{tot} = 2700\,\mathrm{cm}^3$. Vertical entrainment estimates now account for 22% and 30%, respectively, of observed mixed-fluid volumes. These estimates would seem to be upper bounds on the vertical entrainment and support the assumption that horizontal entrainment plays the dominant role.

7. Variations in bar width

The horizontal entrainment model (26) implies that the production of mixed fluid is independent of bar width. This is tested with a series of experiments with variations in bar width $L_B = [15.2, 20.3, 22.9]$ cm, $\frac{1}{2}$, $\frac{2}{3}$, and $\frac{3}{4}$ of the original width, respectively. The range of bar size is based on two considerations: keeping the mixing region small relative to the tank size, and keeping it large relative to the rotational length scale L_f in order to avoid interactions between lateral flows being entrained into the turbulent zone from opposite sides. It is assumed that the properties of turbulent motion, given by (13), are unchanged.

For each bar width, the bar frequency $\omega = 14\,\mathrm{s}^{-1}$ is held constant, and experiments are conducted for three different values of N/f. See table 1, Experiments 16–24. Three experiments, Experiments 25–27, are run without rotation and one without stratification, Experiment 15. The data are analysed as in the earlier experiments.

The mean height of the mixed layer h_m is plotted against the buoyancy height scale H_N (14) in figure 14 along with the earlier results from figure 8. The new data fall within the error limits of the original fit (18), showing that turbulent properties are unaffected by variations in L_B over the range, $\frac{1}{8} \leqslant h_m/L_B \leqslant \frac{1}{3}$.

The rotational length scale L_f, which also depends on the turbulent properties, is examined in an unstratified experiment using the shortest bar width. The measurements of areal spreading are included in figure 12, and scale as $L_f^2 ft$, consistent with the original unstratified data for $L_B = 30.5$ cm.

Mixed-fluid volume observations from the nine new rotating stratified experiments with various L_B are presented in figure 15. Figure 15(a) plots the dimensional data and figure 15(b) plots the data scaled according to (24). The results from the experiments with the $\frac{3}{4}$ width bar are on the low side, but there is no pattern of shorter bar widths generating smaller volumes of mixed fluid. Overall, the best fit for all bar widths is the original horizontal entrainment scaling (24) that is independent of L_B.

8. The limits of rotational effects

The experiments discussed so far have investigated localized mixing in rotating, stratified fluids with $\frac{1}{4} \leqslant N/f \leqslant 2$. They indicate that while local vertical mixing and the height of the mixed layer are independent of rotation, the production of mixed fluid is restricted by it. The restrictive effects of rotation are seen in the lateral spreading (22) and the volume growth (24) of mixed fluid, both of which scale as $f^{-1/2}$. The flux of mixed fluid increases as the rotation rate decreases, but cannot

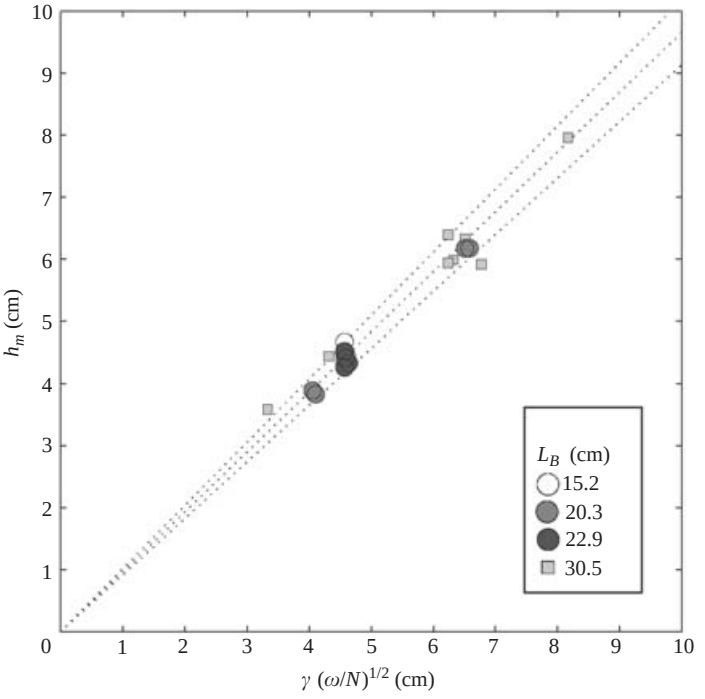

FIGURE 14. Mean height of mixed layer versus buoyancy scale height (14), for experiments with all bar widths. The small squares indicate the original set with $L_B = 30.5$ cm (see figure 8). The dotted lines give the original straight line fit $\pm$ one standard deviation.

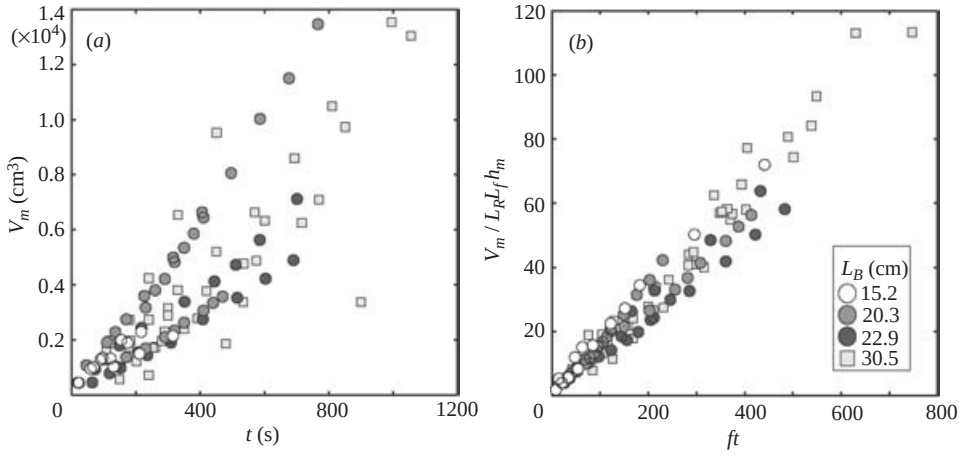

FIGURE 15. Volume of mixed fluid for all bar widths. The squares indicate the original set with $L_B = 30.5$ cm. (*a*) Volume (cm^3) vs time (s). (*b*) Volume normalized by $L_R L_f h_m$ vs non-dimensional time ft, with $L_R = (N/f)h_m$, and L_f and h_m given by (15) and (18), respectively.

grow indefinitely. This section examines the non-rotating limit in order to investigate the behaviour of mixed fluid production as $f \to 0$. The results from six non-rotating stratified experiments are discussed. Three experiments are conducted for the original

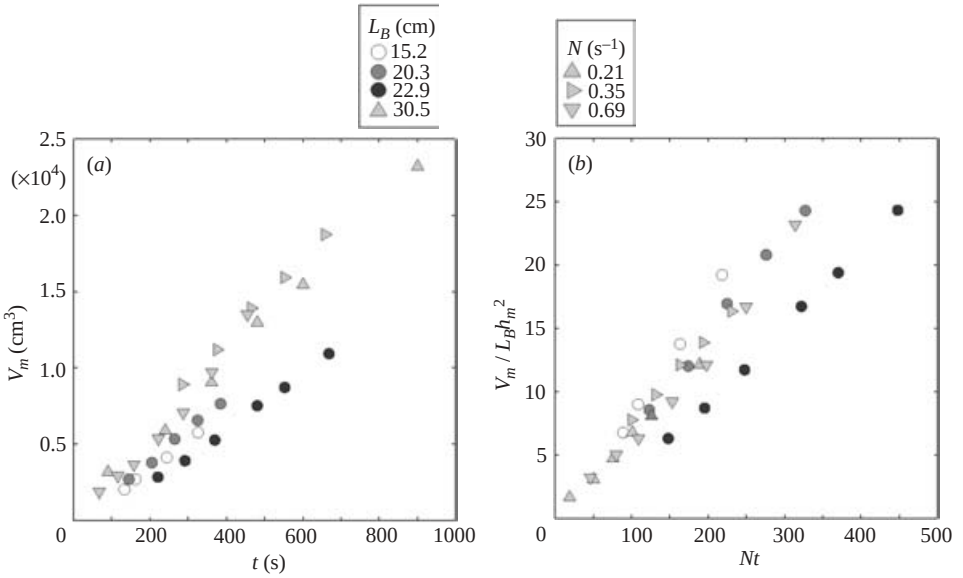

FIGURE 16. Volume of mixed fluid in experiments without rotation. Bar width, L_B, is indicated by the circles. Stratification in the experiments with $L_B = 30.5$ cm is indicated by the triangular shapes. (*a*) Volume (cm^3) vs time (s). (*b*) Volume normalized by $L_B h_m^2$ vs non-dimensional time Nt.

bar $L_B = 30.5$ cm with $N = [0.21, 0.35, 0.69]$ s^{-1}, and one each for the other bar widths $L_B = [15.2, 20.3, 22.9]$ cm with $N = [0.67, 0.85, 0.67]$ s^{-1}, respectively.

The mean mixed-layer heights h_m, immediately in front of the bar, are included in figures 8 and 14 and are indistinguishable from the results of the rotating experiments. However, unlike the rotating experiments the layers do not maintain a uniform height as they move into the interior. In the absence of rotation the turbulent fluid simply collapses into a thinning laminar intrusion of mixed fluid as shown in figure 2(*a*).

The horizontal areas of the spreading fluid are measured as before from the plan views, but the volume estimates are complicated by the non-uniform heights. The volume is estimated using a spatial mean height $\overline{h}$ calculated from the intrusion side-view area and length. This method tends to overestimate the volume as the mixed layer spreads beyond the width of the mixing bar, but other methods of representing h_m, such as fitting triangular and parabolic functions to the intrusion shape, were found to be inconsistent predictors of layer height.

The mixed-fluid volume estimates are shown in figure 16. Figure 16(*a*) plots the dimensional data, and figure 16(*b*) shows the volume scaled by $L_B h_m^2$ versus non-dimensional time Nt. This scaling gives the best fit for all the data, even though the experiment with the $\frac{3}{4}$ width bar falls below the others, just as in the rotating experiments. The experiments for each bar width involve separate laboratory setups and it is possible that different conditions have been unintentionally introduced. If the $\frac{3}{4}$ bar experiment is excluded, a straight line fit to the data gives the volume,

$$V_m = (0.072 \pm 0.008) L_B h_m^2 Nt. \tag{32}$$

With all data included $V_m = (0.064 \pm 0.011) L_B h_m^2 Nt$. The flux Q is constant,

$$Q_{f=0} \propto L_B N h_m^2, \tag{33}$$

and unlike the rotating experiments is a function of the mixing-zone width.

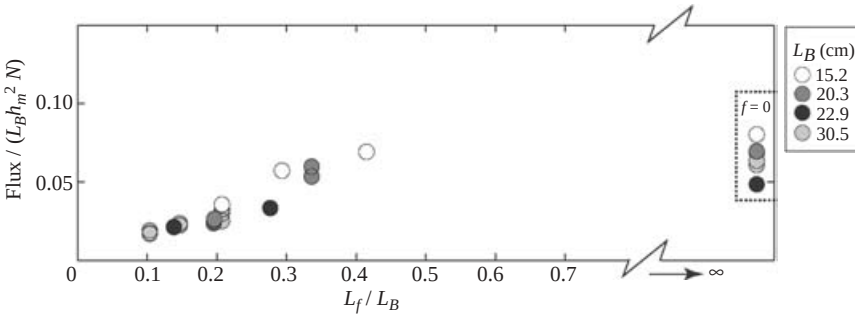

FIGURE 17. Flux of mixed fluid in experiments with and without rotation. The legend indicates the bar width L_B of each experiment. For the rotating experiments flux is normalized by $L_B h_m^2 N t$ and plotted vs L_f/L_B, with L_f and h_m given by (15) and (18), respectively. Flux for the experiments without rotation is plotted on the far right.

The model for mixing in the presence of rotation (§ 6.1) suggests that an appropriate scaling for the non-rotating case could be based on entrainment at the sides of the turbulent zone over an area $h_m h_m$ leading to a volume scaling h_m^3. However, this scaling does not collapse the data as well as the scaling $L_B h_m^2$.

The production of mixed fluid may be driven by the horizontal pressure gradient at the face of the turbulent zone, of width L_B and height h_m, and supplied by a combination of vertical and horizontal entrainment. The vertical entrainment model (§ 6.2) again suggests that vertical entrainment alone is insufficient. The qualitative observations of circulation in the non-rotating experiments indicate the presence of lateral entrainment. Dye traces from potassium permanganate crystals show compensatory return flows of ambient fluid at the level of the mixed layer. These flows may also be supplemented by horizontal flow into the front of the turbulent region along the top and bottom edges of the collapsing intrusion, as described in the experiments of De Silva & Fernando (1998).

Figure 17 compares the production of mixed fluid with and without rotation. The flux Q calculated for each experiment is scaled by $L_B N h_m^2$. The rotating experiments are plotted versus L_f/L_B. Values for the non-rotating experiments, which correspond to $L_f \to \infty$, are placed at the far right of the plot. For a given bar width the flux of mixed fluid in the presence of rotation is always lower than for $f = 0$. The magnitude of flux approaches the non-rotating values as the rotational length scale L_f increases, that is, as rotation decreases. The non-rotating limit appears to be achieved for $L_f/L_B \geqslant 0.4$–0.5. However, there are no data at finite L_f and $L_f/L_B > 0.5$. It is interesting that the factor that differentiates rotating from non-rotating experiments is a function of the rotational length scale and the width of the mixing region rather than N/f as might be have been expected.

9. Discussion

The present experiments on localized turbulence in a rotating stratified fluid indicate that the vertical extent of overturning and the height of the mixed layer are set by stratification and independent of rotation. However, the flux of mixed fluid, which depends primarily on lateral entrainment of unmixed fluid into the turbulent zone, is limited by the rotational control of the turbulence.

The scalings resulting from the laboratory experiments can be written in terms of the external parameters, N, f and ω, using the length scale definitions for H_N,

L_f and L_R, (14)–(16). Thus, as numerous previous investigations have found, mixed-layer height is a decreasing function of the ambient stratification and independent of rotation,

$$h_m \sim \omega^{1/2} N^{-1/2}. \tag{34}$$

The lateral spreading of mixed fluid increases with stratification, decreases with greater rotation, and is linear in time,

$$A_m \sim \omega \left(\frac{N}{f}\right)^{1/2} t. \tag{35}$$

Since with rotation the mixed-layer height is spatially uniform in the coherent portion of the outflow, the exported volume of mixed fluid,

$$V_m = h_m A_m(t) \sim \omega^{3/2} f^{-1/2} t, \tag{36}$$

also grows linearly with time. It is restricted by rotation and, interestingly, is independent of the stratification.

The characteristic dimensions of the mixed fluid are all functions of the bar frequency ω, which represents the imposed turbulence through the parameterization of the inverse turbulent time scale, $u_t/l_t = \gamma^2 \omega d^{-2}$ (13). Increasing ω increases u_t (l_t is independent of ω), thus making the turbulence more energetic. Since in the ocean turbulence is driven by processes, such as internal wave breaking, that are not direct analogues of ω, it is convenient to eliminate ω in favour of h_m, a quantitiy that can be measured or, as discussed below, inferred from observations. This gives the experimentally determined scaling for mixed-fluid flux written in terms of N, f, and h_m,

$$\frac{\mathrm{d}V_m}{\mathrm{d}t} = Q = 0.16 \left(\frac{N}{f}\right)^{3/2} h_m^3 f, \tag{37}$$

and lateral spreading

$$A_m = 0.15 \left(\frac{N}{f}\right)^{3/2} h_m^2 f t. \tag{38}$$

The mixed-layer thickness h_m can be estimated from the Thorpe scale, L_T, a length scale associated with turbulent overturns obtained from a reordering of unstable density inversions in an observed profile (Thorpe 1977). It can also be inferred from the measurement of turbulent properties. The dissipation rate of turbulent kinetic energy, $\varepsilon = u_t^3/l_t$ (6), is related to layer height by the Ozmidov scale, $L_O = (\varepsilon/N^3)^{1/2}$ (5). (See § 3.1) The experiments show $h_m/L_O \approx 4$, giving

$$h_m \approx 4 \left(\frac{\varepsilon}{N^3}\right)^{1/2}. \tag{39}$$

Previous laboratory studies (Thorpe 1982; Browand & Hopfinger 1985; Davies *et al.* 1991; De Silva & Fernando 1998) found values between 1 and 5 for the ratio of critical height to Ozmidov length. A similar relationship was also established in a study of wind-driven mixing in a fresh water lake (Dillon 1982). Dillon used density profiles and microstructure measurements to show that, away from the source of turbulence at the surface, the Thorpe scale was directly proportional to the Ozmidov scale, $L_T \approx 1.25 L_O$.

Site (depth (m))	N (s^{-1})	f (s^{-1})	ε ($m^2 s^{-3}$)	N/f	H_ε (m)
MidAtlantic Ridge crest (4300)	1×10^{-3}	5.4×10^{-5}	1.4×10^{-9}	19	500
MidAtlantic Ridge canyon (4550)	7.7×10^{-4}	5.4×10^{-5}	2×10^{-9}	14	500
Pacific Seamount flank (1300)	2.2×10^{-3}	7.8×10^{-5}	4.5×10^{-9}	29	200
Continental Slope canyon (1100)	1×10^{-3}	8.7×10^{-5}	6×10^{-9}	12	150

TABLE 2. Typical values of the buoyancy frequency N and the dissipation rate of turbulent kinetic energy ε for four ocean sites. Also listed are the Coriolis frequency f, N/f, and the vertical extent of significant dissipation, H_ε.

With the appropriate substitutions, L_f, L_R and the flux Q of mixed fluid are given as functions of N, f and ε:

$$L_f \approx 4 \left(\frac{N}{f}\right)^{1/2} \left(\frac{\varepsilon}{N^3}\right)^{1/2}, \tag{40}$$

$$L_R \approx 4 \left(\frac{N}{f}\right) \left(\frac{\varepsilon}{N^3}\right)^{1/2}, \tag{41}$$

$$Q \approx 10 \left(\frac{N}{f}\right)^{3/2} \left(\frac{\varepsilon}{N^3}\right)^{3/2} f. \tag{42}$$

The coefficients in (39)–(42) depend in part on the specific laboratory mixing mechanism used in the experiments. Even with this caveat in mind, it is worthwhile to apply the scalings. The implications for oceanic boundary mixing are examined using observations at four sites: the crest and canyon of a transverse fracture zone on the MidAtlantic Ridge (Polzin *et al.* 1997; Ledwell *et al.* 2000; St. Laurent, Toole & Schmitt 2001), the flank of the North Pacific Fieberling Seamount (Kunze & Toole 1997; Toole *et al.* 1997), and a canyon on the North Carolina continental slope (K. Polzin, personal communication). Table 2 shows typical values of the buoyancy frequency N and dissipation rate ε for a representative depth at each site. It also gives the Coriolis frequency f, N/f and H_ε, the vertical extent of significant dissipation.

The calculated mixed layer heights (39) are $2.5 \leqslant h_m \leqslant 10$ m. In the one instance where overturning scales are recorded, at the seamount flank, the height, $h_m = 2.5$ m, compares well with the observed scales which are $O(1)$ m and a maximum of 4 m (Toole *et al.* 1997). With $h_m \leqslant 10$ m and $N/f = O(10)$, the deformation radii associated with the exported mixed fluid, $L_R = O(100)$ m, are very small by oceanographic standards. Laboratory results predict that the coherent advance of mixed fluid into the interior will be arrested at length scales equal to approximately $10L_R$. Thus, intrusions are expected to develop baroclinic instabilities within about 1 km of the boundary.

Estimating the total mixed-fluid production is somewhat more problematic since the flux formula (42) is determined for a single isolated patch of mixing and numerous irregularly spaced patches may be generated at the sites listed in table 2. The flux for an individual patch is independent of patch width L_B, at least within the experimental limits, $0.1 \leqslant L_f/L_B \leqslant 0.4$. Given the inferred rotational length scales (40), $15 < L_f < 35$ m, the formula applies to patches between 30 and 350 m wide and predicts a flux, $0.03 \leqslant Q \leqslant 0.50\ m^3/s$. For patch widths < 30 m, i.e. for $L_f/L_B \geqslant 0.4$, the volume flux of mixed fluid is expected to be comparable with the flux observed in the absence of rotation (33) (see figure 17). For patch widths $L_B \gg 350$ m or $L_f/L_B \ll 0.1$,

the laboratory results suggest that vertical entrainment, which is a function of patch width, may become increasingly significant.

These estimates are for individual patches of height h_m. It seems more likely that the scales will depend also on the height of the dissipation region, H_ε. Experimental studies have shown that turbulent mixing over an extended vertical distance produces multiple layers of mixed fluid. The grid mixing experiments of Ivey & Corcos (1982), Thorpe (1982), and Browand & Hopfinger (1985) generated multiple layers, each of which was proportional to the Ozmidov scale. Multiple horizontal intrusions were also observed in the rod stirring experiments of Park, Whitehead & Gnanadeskian (1994), and Perera, Fernando & Boyer (1995) and in laboratory studies of wave breaking on sloping boundaries (Cacchione & Wunsch 1974; Ivey & Nokes 1989). If stacked layers of mixed fluid, exported from the regions of intense dissipation cited in table 2, acted as a single vertically coherent unit with respect to the ambient stratification and rotation, the penetration into the interior would be proportional to the height scale H_ε, which is 15 to 100 times greater than h_m. This would lead to coherent penetration distances of $O(10)$ km and mixed fluid fluxes up to $O(10^4)$ times the estimate for a single layer. The question of the collective behaviour of a number of vertically stacked intrusions in the presence of rotation was not investigated, but it could readily be explored in a future study.

The horizontal distribution of turbulent mixing also requires further investigation. In general, the total production of mixed fluid is expected to depend on the number of discrete patches of mixing rather than on the horizontal extent of rough topography. However, the abrupt features that are assumed to promote patchiness and increase mixed fluid flux may, instead, pose barriers to lateral entrainment and thus decrease production. If localized turbulence is partially enclosed, mixed-fluid production may shift from rotational control to dependence on mixing-region length and vertical entrainment, and outflow patterns may change as well. A second paper will address these issues through a set of experiments that investigate mixing at the closed end of a channel that opens into a larger basin.

In the present set of experiments, the most striking result is the significant role of lateral flows in the production as well as the distribution of mixed fluid. It is not surprising that fluid would preferentially follow isopycnals, but the previous one- and two-dimensional laboratory studies precluded lateral entrainment at the level of the mixing. When the mixing is localized, lateral entrainment can sustain a constant flux of mixed fluid at a much higher rate than can be produced through vertical entrainment alone. The lateral processes also bring out the relationship between rotation and turbulence and demonstrate the inhibiting effects of rotation on mixed-fluid production.

This work was supported by the Ocean Ventures Fund, the Westcott Fund and the WHOI Academic Programs Office. Financial support was also provided by the National Science Foundation through grant OCE-9616949. This is Woods Hole Oceanographic Institution Contribution Number 11120 .

REFERENCES

Barcilon, V. & Pedlosky, J. 1967 On the steady motions produced by a stable stratification in a rapidly rotating fluid. *J. Fluid Mech.* **29**, 673–690.

Browand, F. K. & Hopfinger, E. J. 1985 The inhibition of vertical turbulent scale by stable stratification. In *Turbulence and Diffusion in Stable Environments* (ed. J. C. R. Hunt), pp. 15–27. Oxford University Press.

Cacchione, D. & Wunsch, C. 1974 Experimental study of internal waves over a slope. *J. Fluid Mech.* **66**, 223–239.

Davies, P. A., Fernando, H. J. S., Besley, P. & Simpson, R. J. 1991 Generation and spreading of a turbulent mixed layer in a rotating, stratified fluid. *J. Geophys. Res.* **96**, 12567–12585.

Denton, R. A. & Wood, I. 1981 Penetrative convection at low Péclet number. *J. Fluid Mech.* **113**, 1–21.

De Silva, I. P. D. & Fernando, H. J. S. 1998 Experiments on collapsing turbulent regions in stratified fluids. *J. Fluid Mech.* **358**, 29–60.

Dickinson, S. C. & Long, R. R. 1983 Oscillating-grid turbulence including effects of rotation. *J. Fluid Mech.* **126**, 315–333.

Dillon, T. M. 1982 Vertical overturns: A comparison of Thorpe and Ozmidov length scales. *J. Geophys. Res.* **87**, 9601–9613.

Fernando, H. J. S. 1988 The growth of a turbulent patch in a stratified fluid. *J. Fluid Mech.* **190**, 55–70.

Fleury, M., Mory, M., Hopfinger, E. J. & Auchere, D. 1991 Effects of rotation on turbulent mixing across a density interface. *J. Fluid Mech.* **223**, 165–191.

Hogg, N., Biscaye, P., Gardner, W. & Schmitz, Jr. W. J. 1982 On the transport and modification of Antarctic Bottom Water in the Vema Channel. *J. Mar. Res.* **40** (Suppl), 231–263.

Hopfinger, E. J., Browand, F. K. & Gagne, Y. 1982 Turbulence and waves in a rotating tank. *J. Fluid Mech.* **125**, 505–534.

Hopfinger, E. J. & Toly, J.-A. 1976 Spatially decaying turbulence and its relation to mixing across density interfaces. *J. Fluid Mech.* **78**, 155–175.

Ivey, G. N. 1987 Boundary mixing in a rotating, stratified fluid. *J. Fluid Mech.* **183**, 25–44.

Ivey, G. N. & Corcos, G. M. 1982 Boundary mixing in a stratified fluid. *J. Fluid Mech.* **121**, 1–26.

Ivey, G. N. & Nokes, R. L. 1989 Vertical mixing due to breaking of critical internal waves on sloping boundaries. *J. Fluid Mech.* **204**, 479–500.

Kunze, E. & Toole, J. M. 1997 Tidally driven vorticity, diurnal shear, and turbulence atop Fieberling Seamount. *J. Phys. Oceanogr.* **27**, 2663–2693.

Ledwell, J. R., Montgomery, E. T., Polzin, K. L., St. Laurent, L. C., Schmitt, R. W. & Toole, J. M. 2000 Evidence for enhanced mixing over rough topography in the abyssal ocean. *Nature* **403**, 179–182.

Linden, P. F. 1973 The interaction of a vortex ring in a sharp density interface: a model for turbulent entrainment. *J. Fluid Mech.* **60**, 467–480.

Lueck, R. G. & Mudge, T. D. 1997 Topographically induced mixing around a shallow seamount. *Science* **276**, 1831–1833.

Maxworthy, T. & Monismith, S. G. 1988 Differential mixing in a stratified fluid. *J. Fluid Mech.* **189**, 571–598.

Munk, W. 1966 Abyssal recipes. *Deep-Sea Res.* **13**, 707–730.

Munk, W. & Wunsch, C. 1998 Abyssal recipes II: energetics of tidal and wind mixing. *Deep-Sea Res.* I **45**, 1977–2010.

Oster, G. 1965 Density gradients. *Sci. Am.* **213**, 70–76.

Ozmidov, R. V. 1965 On the turbulent exchange in a stably stratified ocean. *Izv. Atmos. Oceanic Phys.* (Engl. Transl.) **1**, 493–497.

Park, Y.-G., Whitehead, J. A. & Gnanadeskian, A. 1994 Turbulent mixing in stratified fluids: layer formation and energetics. *J. Fluid Mech.* **279**, 279–311.

Perera, M. J. A. M., Fernando, H. J. S. & Boyer, D. L. 1995 Mixing induced by oscillatory stratified flow past a right-circular cylinder. *J. Fluid Mech.* **284**, 1–21.

Polzin, K. L., Toole, J. M., Ledwell, J. R. & Schmitt, R. W. 1997 Spatial variability of turbulent mixing in the abyssal ocean. *Science* **276**, 93–96.

St. Laurent, L. C., Toole, J. M. & Schmitt, R. W. 2001 Buoyancy forcing by turbulence above rough topography in the abyssal Brazil Basin. *J. Phys. Oceanogr.* **31**, 3476–3495.

Thomas, P. J. & Linden, P. F 1996 A laboratory simulation of mixing across tidal fronts. *J. Fluid Mech.* **309**, 321–344.

Thorpe, S. A. 1977 Turbulence and mixing in a Scottish Loch. *Phil. Trans. R. Soc. Lond.* A **286**, 125–181.

Thorpe, S. A. 1982 On the layers produced by rapidly oscillating a vertical grid in a uniformly stratified fluid. *J. Fluid Mech.* **124**, 391–409.

Toole, J. M., Polzin, K. L. & Schmitt, R. W. 1994 Estimates of diapycnal mixing in the abyssal ocean. *Science* **264**, 1120–1123.

Toole, J. M., Schmitt, R. W. & Polzin, K. L. 1997 Near-boundary mixing above the flanks of a midlatitude seamount. *J. Geophys. Res.* **102**, 947–959.

Turner, J. S. 1973 Mixing across density interfaces. In *Buoyancy Effects in Fluids*, pp. 288–312. Cambridge University Press.

Turner, J. S. 1986 Turbulent entrainment: the development of the entrainment assumption, and its application to geophysical flows. *J. Fluid Mech.* **173**, 431–471.

Wells, J. R. 2003 A laboratory study of localized boundary mixing in a rotating stratified fluid. PhD dissertation, MIT-WHOI Joint Program in Oceanography.